SECURITY CLASSIFICATION OF THIS PAGE

UMENTATION PAGE

Form Approved
OMB No 0704-0188

1. AD-A265 552

1b. RESTRICTIVE MARKINGS

2a.

3. DISTRIBUTION / AVAILABILITY OF REPORT
APPROVED FOR PUBLIC RELEASE
DISTRIBUTION UNLIMITED

2b. DECLASSIFICATION / DOWNGRADING SCHEDULE

4. PERFORMING ORGANIZATION REPORT NUMBER(S)
VPI-AOE-201

5. MONITORING ORGANIZATION REPORT NUMBER(S)

6a. NAME OF PERFORMING ORGANIZATION
Aerospace and Ocean Engineering Department

6b. OFFICE SYMBOL (If applicable)

7a. NAME OF MONITORING ORGANIZATION
Office of Naval Research

6c. ADDRESS (City, State, and ZIP Code)
Virginia Polytechnic Institute and State Univ., Blacksburg, VA 24061-0203

7b. ADDRESS (City, State, and ZIP Code)
800 N. Quincy St.
Arlington, VA 22217

8a. NAME OF FUNDING / SPONSORING ORGANIZATION
Office of Naval Research

8b. OFFICE SYMBOL (If applicable)

9. PROCUREMENT INSTRUMENT IDENTIFICATION NUMBER
N00014-92-J-1292

8c. ADDRESS (City, State, and ZIP Code)
800 N. Quincy Street
Arlington, VA 22217

10. SOURCE OF FUNDING NUMBERS

PROGRAM ELEMENT NO.	PROJECT NO.	TASK NO	WORK UNIT ACCESSION NO

93-12952

11. TITLE (Include Security Classification)
Development of the One-Component Diode-Array Velocimeter

12. PERSONAL AUTHOR(S)
William J. Devenport and Edward J. Smith

13a. TYPE OF REPORT	13b. TIME COVERED	14. DATE OF REPORT (Year, Month, Day)	15. PAGE COUNT
Final Technical	FROM 1/1/92 TO 3/31/93	June 1993	89

16. SUPPLEMENTARY NOTATION

93 6 00 053

17. COSATI CODES			18. SUBJECT TERMS (Continue on reverse if necessary and identify by block number)
FIELD	GROUP	SUB-GROUP	Flow Measurement, Laser Turbulance

19. ABSTRACT (Continue on reverse if necessary and identify by block number)

A new optical flow measurement technique, the diode array velocimeter, has been proposed. A DAV works by timing the passage of seed particles through a small section of a light beam. This is achieved by imaging light scattered by the particles on to one or more photodiode arrays. The arrays have a few carefully shaped elements, the shapes and positions of the elements being used to control the measurement volume geometry and thus select the measurement made. Measurement volumes sensitive to velocity, position and acceleration may be designed. Measurements in highly turbulent and reversing flows are possible.

A DAV for one-component velocity measurements has been developed to demonstrate this concept. This device uses a single laser beam to illuminate particles and a photodiode array with two rectangular elements to sense their motion. The sensitivity of this device to electrical noise in the photodiode circuitry is analyzed and found to decrease with

20. DISTRIBUTION / AVAILABILITY OF ABSTRACT
☒ UNCLASSIFIED/UNLIMITED ☐ SAME AS RPT ☐ DTIC USERS

21. ABSTRACT SECURITY CLASSIFICATION

22a. NAME OF RESPONSIBLE INDIVIDUAL

22b. TELEPHONE (Include Area Code)

22c. OFFICE SYMBOL

DD Form 1473, JUN 86 Previous editions are obsolete. SECURITY CLASSIFICATION OF THIS PAGE

DTIC ELECTE JUN 10 1993 S E D

reduction in measurement volume size. The angle response is also studied and, depending on the signal processing used, found to be closely cosinusoidal to about 60°. Changes to the photodiode array design could substantially increase this limit.

Measurements of mean velocity, normal turbulence stress and velocity skewness made with this DAV in two attached boundary layer flows compare favorably with hot-wire measurements. Useful DAV measurements were made as close as 0.2mm from the wall. DAV measurements made in a separated flow formed downstream of a fence are also presented. These show all expected features of the separated shear layer and recirculation including the sub-boundary layer formed beneath the backflow. Histograms measured in the reversing part of this flow show a hole near zero velocity that is a consequence of the imperfections in the DAV angle response and the limitations on the maximum measured transit time. These are not fundamental problems, however, and the hole could be minimized or eliminated by using a different photodiode array design and measurement strategy.

DEVELOPMENT OF THE ONE-COMPONENT DIODE-ARRAY VELOCIMETER

Final report to the Office of Naval Research
for work performed under grant number N00014-92-J-1292
for the period ending 31st March 1993

by

William J. Devenport and Edward J. Smith,
Department of Aerospace and Ocean Engineering,
Virginia Polytechnic Institute and State University,
Blacksburg, Virginia 24061, U.S.A.

Report VPI-AOE-201

ABSTRACT

A new optical flow measurement technique, the diode array velocimeter, has been proposed. A DAV works by timing the passage of seed particles through a small section of a light beam. This is achieved by imaging light scattered by the particles on to one or more photodiode arrays. The arrays have a few carefully shaped elements, the shapes and positions of the elements being used to control the measurement volume geometry and thus select the measurement made. Measurement volumes sensitive to velocity, position and acceleration may be designed. Measurements in highly turbulent and reversing flows are possible.

A DAV for one-component velocity measurements has been developed to demonstrate this concept. This device uses a single laser beam to illuminate particles and a photodiode array with two rectangular elements to sense their motion. The sensitivity of this device to electrical noise in the photodiode circuitry is analyzed and found to decrease with reduction in measurement volume size. The angle response is also studied and, depending on the signal processing used, found to be closely cosinusoidal to about 60°. Changes to the photodiode array design could substantially increase this limit.

Measurements of mean velocity, normal turbulence stress and velocity skewness made with this DAV in two attached boundary layer flows compare favorably with hot-wire measurements. Useful DAV measurements were made as close as 0.2mm from the wall. DAV measurements made in a separated flow formed downstream of a fence are

also presented. These show all expected features of the separated shear layer and recirculation including the sub-boundary layer formed beneath the backflow. Histograms measured in the reversing part of this flow show a hole near zero velocity that is a consequence of the imperfections in the DAV angle response and the limitations on the maximum measured transit time. These are not fundamental problems, however, and the hole could be minimized or eliminated by using a different photodiode array design and measurement strategy.

CONTENTS

1. INTRODUCTION

This report describes an optical measurement technique for turbulent flows - the diode array velocimeter, or DAV. The simplest possible optical layout for a DAV is shown in figure 1. A single light beam is directed into a flow. Particles in the flow, either naturally occurring or artificially introduced, scatter light as they pass through the beam. Scattered light from a small section of the beam is collected by a lens and focussed onto a photodiode array with a few carefully shaped elements. As particles pass through the beam their images pass across the array elements. Measurements are made by timing this passage.

The measurement volume implied by this optical arrangement is the intersection of the light beam and the projection of the photodiode array elements back through the receiving lens. By controlling the number, shape and position of the elements, the beam size and the receiving lens orientation and magnification, a wide variety of measurement volume geometries may be generated. For example, consider the photodiode array of figure 2 mounted in the optical system of figure 1 with its long axis parallel to the beam. This would produce a measurement volume consisting of the two parallel 'plates' shown in figure 3, suitable for one-component velocity measurements. The measurement volume could be made very small by focussing the laser beam and using a high receiving lens magnification. In principle, measurement volumes sensitive to particle position and acceleration may be similarly designed. By using more than one photodiode array and/or

more than one receiving lens, simultaneous two and three component measurements should also be possible.

The idea of using a single beam or an array of detectors in an anemometer is not new. For example, Boutier and Lefevre (1988) used an array of optical fibers and a series of photo-multiplier tubes to detect velocities with a single laser beam. Hirleman at al. (1984) used only one detector and one beam, the transit time of particles through the laser beam being measured. Detector arrays have been used in some laser-two-focus systems (see for example Ohmura et al. (1992)). The drawback of all these types of schemes has been their poor accuracy when compared to laser Doppler velocimetry.

What is new about the DAV concept is its use of photodiode array geometry, the shapes of the elements as well as their positions being exploited to select the form of the measurement volume and thus the measurement made. Silicon photodiode arrays can be made in almost any shape and pattern and are therefore well suited to this application.

In velocity measurements the DAV has, at least in principle, some significant advantages over competing techniques such as laser Doppler anemometry (LDA) and laser-two-focus anemometry. Compared to laser Doppler anemometry the DAV is simple, requiring only one (not-necessarily coherent or monochromatic) illuminating beam regardless of the number of components to be measured. In addition the signals it produces (electrical pulses indicating the passage of a particle image over a photodiode element) are easier and cheaper to process than frequency-modulated bursts. Optical simplicity is also an advantage in comparison to laser-two-focus anemometry. So are

accuracy and the ability to make velocity measurements regardless of turbulence level and flow reversais.

This report describes the design and construction of a DAV for one-component velocity measurements. This system is analyzed and its performance in attached and separated flows examined. The primary objective of this work was to demonstrate the viability of the DAV concept.

2. DESIGN OF THE ONE-COMPONENT DAV

2.1 Optical system

The optical system of a one-component DAV is in principle very simple. All that is required is a collimated light source (which need not be coherent or monochromatic), a receiving lens and a photodiode array. As the light source we used a Spectra Physics model 164 argon-ion laser, since this was already available. At a wavelength of 514.5nm it produced a 1W beam with a Gaussian intensity distribution. As the receiving lens we chose an Oriel Corporation 50mm-diameter, 100mm focal length achromat, based on its low cost, ability to collect a reasonable solid angle of scattered light and form a high-quality image. The photodiode array chosen was the Silicon Detector Corporation SD160, illustrated in figure 2. It consists of two rectangular PIN photodiode elements, each 4.57x0.51mm, placed side by side and separated by a distance of 0.02mm. As will be discussed later this geometry, while adequate, is not the best possible for a one-component DAV. The SD160 was chosen because was the most suitable device already in commercial production[1].

In addition to these essential components, an Oriel model 15261 beam expander and 10μm spatial filter was used to vary the diameter of the laser beam and ensure its Gaussian intensity distribution in the measurement volume. A 12.7-mm wide slit, placed

[1]Building a PIN photodiode array to a new design initially costs between $10,000 and $20,000. Subsequent devices of the same design, however, typically cost $50 to $100 each.

adjacent to the receiving lens and aligned with the long axis of the detector, was used to improve depth of focus. Several front surface mirrors were also used to position the beam. A schematic of the optical system is shown in figure 4. All optical components were mounted on an aluminum table built into the top of a milling machine base. The table could be positioned using a three-axis traverse installed in the base.

With its components fixed, design of the optical system involved only three variables; (i) the laser beam diameter, (ii) the angle of the receiving lens axis to the laser beam (the receiver angle) and, (iii) the distance of the receiving lens from the beam (i.e. the optical magnification M of scattering particle images). The beam diameter (0.4mm at the $1/e^2$ points) and optical magnification (x10) were chosen as a consequence of design constraints described in the following sections. The receiver angle was fixed at 90° to give the simplest possible measurement volume shape. The measurement volume (figure 3) is the region within the laser beam where light scattered by seeding particles arrives at one of the photodiode elements. It therefore consists of two thin rectangular regions of space side by side. Its length (h=.457mm), overall width (D=.104mm) and separation of its two halves (d=.002mm) are equal to the corresponding dimensions of the photodiode array divided by the magnification of the receiving lens. Its depth is the diameter of the laser beam.

2.2 Obtaining signals from the photodiode array

With a constant voltage across them PIN photodiodes convert light power to a

proportional current. The sensitivity of the elements of the SD160 is about 0.2 A/W at 514.5nm. One would therefore expect, given the results of Mie scattering calculations and the available laser power, currents typically of tens of nanoAmps to be generated by the passage of a single particle image across an element of the detector. An amplifier circuit with a net current-to-voltage gain of about $10^7\Omega$ is needed to convert these into usable voltage signals.

Two circuits of the type shown in figure 5 was used to provide this gain separately for the two photodiode elements. In each, the photodiode element is connected between the virtual ground of a high-speed operational amplifier and a reference voltage. A precision, low-capacitance 7MΩ resistor, placed in the feedback loop of the op amp gives a current to voltage gain of $7x10^6$.

The dynamic characteristics of these circuits were determined by simultaneously exciting both photodiodes with a green light emitting diode of flat frequency response (Hewlett Packard HPMP-3507). The results, plotted in figure 6, show the circuits to be closely matched, both having 3dB points at around 140kHz. The frequency response of this type of circuit is limited by stray capacitance across the feedback resistor of the first amplifier, this acting to reduce the feedback impedance at higher frequencies. The output noise level was about $1.5mV_{rms}$ for both circuits.

Figure 7 shows typical DAV signals output from the amplifiers over a range of flow conditions. Note that the origins of the voltage scales in this figure are arbitrary. These signals are formed as follows. A particle, moving at constant speed through the

Gaussian laser beam produces an image in the receiving lens whose light power varies as a Gaussian with time. As the image crosses the photo-diode array each element detects a portion of this Gaussian. The detection and amplification of these signals filters them and adds noise. Note that, since the particle may enter the measurement volume at any angle and not pass through the beam center the photodiode elements may see unsymmetrical portions of the Gaussian (see for example figures 7c and e).

2.3 Timing

The above system was used to measure the magnitude and sign of the instantaneous velocity component u, see figure 3. To do this the transit time of particles between the centers of the measurement volume 'plates' must be extracted from the amplifier output signals. Two different methods for determining the transit time were investigated. The first method involves cross-correlating the signals and then measuring the time delay of the peak correlation coefficient. The second method involves comparing the signals to a trigger level set just above the noise. The time at which each signal crosses the trigger level is recorded. The time difference is then taken as the transit time.

As will be shown in the following sections the correlation scheme has some desirable characteristics. The trigger scheme has the advantage that it could be performed entirely using a simple, purpose built, electronic circuit that could easily be miniaturized. Its primary disadvantage, however, is a greater sensitivity to noise since the transit time is determined only from small parts of the signals.

3. THEORETICAL ANALYSES

3.1 Influence of noise in determining velocity

The relationship between the transit time t determined from the DAV signals and the velocity u inferred from it is ideally

$$u = \frac{A}{t} \tag{1}$$

where A is the distance between the centers of the measurement volume plates (D+d)/2, see figure 3. This measured transit time may be thought of as having a contributions from the actual transit time and electrical noise t'_n. Over a sequence of many samples the actual transit time may be thought of as being made up of a mean T and a fluctuation t'_t associated with unsteadiness in the flow. We may therefore write

$$u = \frac{A}{T+t'_t+t'_n} \tag{2}$$

As indicated t'_n would not be expected to have a mean value. It is simple to show that, to a first order approximation assuming $t'_n << T$ and $t' << T$, equation 2 leads to the expressions

$$U = \frac{A}{T} \tag{3}$$

$$\frac{\overline{u'^2}}{U^2} = \frac{\overline{t'^2_t} + \overline{t'^2_n}}{T^2} = \left(\overline{t'^2_t} + \overline{t'^2_n}\right)\frac{U^2}{A^2} \tag{4}$$

where U and u' represent the measured mean velocity and velocity fluctuation respectively. So, assuming constant $\overline{t'^2_n}$, the influence of electrical noise on normalized turbulence stress measurements should increase as the square of the mean velocity. Obviously minimizing electrical noise is important if accurate turbulence measurements are desired.

Whether the transit time is being determined using a cross-correlation or trigger scheme we would expect the r.m.s. of t'_n to rise if the electrical signal to noise ratio S (peak signal voltage divided by r.m.s. voltage noise level) were decreased. We would also expect it to rise if the amplifier cutoff frequency ω_c were reduced since this would lead to greater filtering of the signals, blurring their definition in time. As shown in the appendix, it follows that

$$\frac{\sqrt{\overline{i_n^2}}}{T} \sim \frac{1}{S\omega_c T} \tag{5}$$

Since the voltage noise in the DAV outputs is independent of signal, S depends only on the peak signal magnitude. This, in turn, will vary linearly with the total light power received in a particle image, which is proportional to the intensity of the laser beam multiplied by the solid angle over which the receiving lens collects light. Using f_1 and l to denote the distance from the measurement volume to the receiving lens and the diameter of that lens respectively, we therefore have,

$$S \sim \frac{P}{\sigma^2}\frac{l^2}{f_1^2} = \frac{P}{\sigma^2 f^{\#2}}\left(\frac{M}{M+1}\right)^2 \tag{6}$$

where P is the total laser beam power, σ is its r.m.s. width, $f^{\#}$ is the f-number of the receiving lens (focal length over diameter) and M is the image magnification it produces. To proceed further we must recognize that there is a linkage between the beam width and the optical magnification of the receiving lens. If the measurement volume geometry is to remain constant then we must have

$$\sigma \sim \frac{1}{M} \tag{7}$$

and so,

$$S \sim \frac{P}{f^{\#2}} \frac{M^4}{(M+1)^2} \tag{8}$$

Substituting this back into equation 5 gives

$$\frac{\sqrt{t'^2_n}}{T} \sim \frac{f^{\#2}(1+M)^2}{PM^4} \frac{1}{\omega_c T} \tag{9}$$

For a given flow velocity, the average transit time T is inversely proportional to M, since optical magnification amplifies the speed of the particle image as well as its size and so, finally, we have

$$\frac{\sqrt{t'^2_n}}{T} \sim \left(\frac{f^{\#2}}{P\omega_c}\right)\left(\frac{(M+1)^2}{M^3}\right) \tag{10}$$

Note that the first term on the right hand side of equation 10 is fixed by the choice of optical and electrical components. To minimize the influence of noise on transit time measurements the receiving lens magnification should therefore be maximized and the laser beam diameter correspondingly reduced. These measures have the added benefits of minimizing the measurement volume size and maximizing signal to noise ratio (making

the presence of a signal much easier to detect).

For the present DAV, M was set at 10, this being the maximum that could be achieved within the available length of optical table. In fixing the aperture, and therefore the f# of the receiving lens, depth of focus was found to be an important consideration. If particle images are out of focus this increases their radius, smoothing the rising and falling edges of the output signals. The net effect is similar to that of a decrease in ω_c. Focussing of particle images in the direction normal to the long axis of the photodiode array was improved by using the 12.7-mm wide slit shown in figure 4.

3.2 Linearity and angle response

Linearity and angle response were studied by simulating signals produced by the DAV over a range of conditions. Consider the measurement volume shown in figure 3. Taking the laser beam as Gaussian we may write its normalized intensity distribution I as

$$I(x,y) = \exp\left(-\frac{x^2+y^2}{2\sigma^2}\right) \tag{11}$$

where σ is the r.m.s. beam width (one quarter of its $1/e^2$ diameter) and the coordinate system (x,y,z) is centered in the measurement volume with the z axis parallel to the beam (figure 3).

Consider a particle with a velocity (u,v,w) moving along a trajectory that crosses the measurement volume center plane at the location $(0,y_o,z_o)$. The particle will experience a light intensity equal to

$$\exp\left(-\frac{x^2+(y+y_0)^2}{2\sigma^2}\right) \tag{12}$$

which may be rewritten in terms of time t as

$$\exp\left(-\frac{(ut)^2+(vt+y_0)^2}{2\sigma^2}\right) \tag{13}$$

Assuming the intensity of light scattered by the particle is proportional to that incident upon it and that the diameter of the particle and its image are negligible, equation 13 may also be used to represent the normalized light intensity received or current signals produced by the photodiode elements. All that is needed are to state the limits of the signal for each element. These are,

for element 1: $-D/2 < ut < -d/2, \quad -h/2 < wt+z_0 < h/2$

for element 2: $d/2 < ut < D/2, \quad -h/2 < wt+z_0 < h/2$

where d, D and h are the dimensions of the measurement volume defined in figure 3. Introducing q to denote the magnitude of the velocity vector $\sqrt{u^2+v^2+w^2}$, angles α and

β to denote its direction (see figure 3) and the non-dimensional variable $t^*=qt/\sigma$, these current signals may be re-written as

$$i(t^*) = \exp\left(-\frac{1}{2}(t^*\cos\alpha)^2 - \frac{1}{2}(t^*\sin\alpha\sin\beta + y_0/\sigma)^2\right) \tag{14}$$

for element 1: $\begin{cases} -D/2\sigma < t^*\cos\alpha < -d/2\sigma \\ -h/2\sigma < t^*\sin\alpha\cos\beta + z_0/\sigma < h/2\sigma \end{cases}$

for element 2: $\begin{cases} d/2\sigma < t^*\cos\alpha < D/2\sigma \\ -h/2\sigma < t^*\sin\alpha\cos\beta + z_0/\sigma < h/2\sigma \end{cases}$

The current to voltage converters amplify and filter these signals. We may write the amplifier output as

$$v(t) = i(t) * h(t\omega_c) \tag{15}$$

where $h(\omega_c t)$ is the amplifier impulse response, ω_c is the angular cutoff frequency of that response and the asterisk denotes convolution. Non-dimensionalizing gives

$$v(t^*) = i(t^*) * h(\omega_c^* t^*) \tag{16}$$

where $\omega_c^* = \omega_c\sigma/q$.

A computer program was written to generate one-component DAV signals for a range of conditions using the above expressions. The signals were generated as records

256 points long. The impulse response required in equation 16 was taken as that of a single pole low-pass filter. The measurement process was then simulated by applying the cross-correlation or trigger timing schemes described above. The velocity inferred from these schemes was then compared to the velocity input to the calculation and the errors calculated.

3.2.1 Cross-correlation scheme.

To interpolate the location of the peak in the cross correlation coefficient function, a 7 point least-squares parabola was used. Peak cross-correlation coefficients were typically greater than 0.99, except for very large flow angles.

We begin by presenting calculations for the correlation scheme applied to the present DAV for which $D/\sigma = 1.04$, $h/D = 4.39$ and $d/D = 0.02$. Figure 8 illustrates the response to a uniform flow at zero yaw and pitch ($\alpha=0$, $\beta=0$). Note that, for this special case, the response is not a function of y_o and z_o. Computed over actual velocity (u_{dav}/q) is plotted as a function of the parameter ω_c^*, which varies inversely with the absolute flow speed. For the present DAV, $\sigma = 0.1$mm and $\omega_c = 2\pi$ x 140,000 giving, for example, $\omega_c^* = 0.5$ at 176/s and 50 at 1.76m/s. Figure 8 shows the DAV output to be closely linear, u_{dav}/q varying only slightly with ω_c^* from 1.024 at $\omega_c^*=0.5$ to 1.006 at $\omega_c^*= 50$. The fact that this ratio is larger than unity implies that the cross-correlation scheme slightly underestimates the actual transit time. For most applications the variation in the ratio would be insignificant, so this effect can be accounted for simply by adjusting

measured velocities by a small constant factor.

Figure 9 shows the response of the DAV in pure pitch (β = 90°) for ω_c^*=5.65 (15.6 m/s). As can be seen from equation 14 the pitch characteristic will in general be a function of y_o. Rather than presenting curves for many different y_o values it is more informative to show the mean response (indicated by the points in figure 9) and its r.m.s. variation over the measurement volume (shown by the error bars). For these averages the y-limits of the measurement volume were taken to be $\pm 2\sigma$ (i.e. the $1/e^2$ points). Ideally the mean variation would be a cosine. Between about $\pm$65° it is, and r.m.s. variations are small. At flow angles greater than 70°, however, the mean curve departs significantly from a cosine and r.m.s. variations increase.

Figure 9 also shows the response in pure yaw (β = 0°) for ω_c^*=5.65. In this case the response is a function of z_o so spatially averaged mean and r.m.s. values are again presented. Clearly the yaw response is unacceptable, the r.m.s. variations being far too large. The reason for the poor performance is simply that at large yaw angles or large z_0, particle images start to cross the ends of the photodiode elements rather than their long edges. The best way to improve the response, without changing the photodiode array geometry, is to ignore the signals produced by these images. This can be done to a certain extent using the magnitude of the peak cross correlation coefficient. While this is close to unity for particles images that cross only the long edges of the diode elements it is much smaller for most of those crossing the ends. Setting a minimum acceptable peak correlation coefficient of course also influences the pitch characteristic.

Figures 10a through d show pitch and yaw characteristics for a minimum peak correlation coefficient of 0.95. Curves for $\omega_c^* = 2.83, 5.65, 11.3$ and 22.6, corresponding to 31, 15.6, 7.8 and 3.9m/s respectively, are presented. The yaw response is greatly improved by this measure, the mean being cosinusoidal up to $\pm 75°$ and the r.m.s. remaining acceptably small, regardless of ω_c^*. For angles less than about 65° the pitch response appears unaltered and largely independent of ω_c^*. For greater angles, however, it is eliminated. As is obvious from this figure the price paid for the improvement in yaw response is that the DAV becomes biased against higher flow angles. This is shown in more detail in figure 11 where the proportion of the measurement volume sensitive to a particular flow angle is plotted vs. flow angle. For the pitch response this proportion remains unity over almost the entire angle range. For yaw, the proportion drops more gradually with increase in angle. However, most of the loss still comes at angles greater than 60°.

While the angle response of the present DAV may not be ideal it is important to remember that it has been achieved using a photodiode array not actually designed for the present purpose. Even if the design is restricted to two rectangular elements, the response can be substantially improved by increasing the aspect ratio of the array h/D and reducing the measurement volume to beam size ratio D/σ. For example, figure 12 shows the angle response for $h/D=17.6$, $D/\sigma=0.52$ and $d/D=.02$ with a minimum peak correlation coefficient of 0.9. The mean pitch and yaw response are nearly perfect cosines to 75 and 85° respectively while r.m.s. variations remain small. The angle bias (figure 11) and non-

linearity (figure 8) are also substantially reduced.

3.2.2 Trigger scheme

To apply the trigger scheme to the model signals requires that a trigger level be set. The natural way to express the trigger level is relative to unity in equation 14. In this context, unity is the normalized output voltage level that would be produced by a stationary particle at the center of the laser beam, if the image of that particle were to lie on one of the photodiode elements. In other words, the trigger level is non-dimensionalized on the maximum possible signal magnitude. This is a constant in both calculation and experiment.

Figure 13 shows the linearity of the trigger scheme for the present DAV ($D/\sigma=1.04$, $h/D=4.39$ and $d/D=0.02$) in a uniform flow of zero yaw and pitch ($\alpha=0$, $\beta=0$) for trigger levels of 0.1, 0.2 and 0.5. In contrast with the correlation scheme, this response is a function of y_o since the absolute magnitude of the signals relative to the trigger level is important. Spatially averaged mean and r.m.s. values are therefore presented as is the proportion of the measurement volume sensitive to each flow velocity.

For a trigger level of 0.1 the linearity appears good, the ratio of measured to actual velocity varying by no more than $\pm 1.3\%$ over the entire range of ω_c, most of this change occurring below $\omega_c=10$. The r.m.s. variation in measured velocity over the measurement volume is also fairly small in this case, remaining less than 1.4%. Increasing the trigger level to 0.3 and then 0.5 increases the absolute error in measured velocity but does not

increase their variation with ω_c. The r.m.s. variation also rises, exceeding 4% at large ω_c for a trigger level of 0.5. The sensitive proportion of the measurement volume is in all cases constant above a small value of ω_c , and thus, in this range fluctuating velocity measurements will be unbiased. This threshold in ω_c increases with trigger level, its maximum value being about 6 for a trigger level of 0.5.t

Figure 14 shows the response to pure pitch and pure yaw for ω_c=5.65 (15.6m/s). For the trigger scheme the pitch characteristic is a function of y_o and the yaw characteristic a function of both y_o and z_o, so spatially averaged mean and r.m.s. values are again presented. Both curves are obviously unacceptable, the r.m.s.variations becoming very large for angles greater than a few degrees.

There are two reasons for this poor performance. The first of these is that particles passing different distances from the center of the laser beam (i.e. at different y_o's) produce signals of widely varying magnitude, all of which are compared to the same trigger level. As a consequence a significant proportion of signals trigger not on their rising edges but near their maxima where the gradient of voltage with time is very small and the shapes of the signals produced by the left and right photodiode elements may be quite different. An obvious solution to this problem is to accept only measurements on signals whose peak magnitude exceeds a certain discrimination level, set somewhere above the trigger level. The results of applying this measure are shown in the pitch and yaw response curves of figure 15. These curves are for a trigger level of 0.1 and a discrimination level of 0.5, the discrimination level actually being applied to the sum of

the signals from the two photodiodes (this is simpler than applying the level separately to the two signals and has almost the same effect). While the pitch response now appears acceptable and the linearity is improved (figure 13), r.m.s variations in the yaw response are still far too large. As with the cross correlation scheme this remaining error is primarily due to particle images crossing the ends of the photodiode elements. However, unlike the cross-correlation scheme, triggering offers no simple way of eliminating these signals. We therefore conclude that, for this particular photodiode array design, triggering cannot produce accurate velocity measurements in most flows.

Fortunately, this is not true in general. It is simple to design other photodiode arrays for which the triggering scheme is accurate. Consider, for example, the photodiode array of figure 16. This is basically the same as the SD160 except that the rectangular elements have been narrowed slightly to allow a smaller rectangular element to be placed between them. This central element is used to distinguish between those particle images which cross the central 25% of the array and those which don't. By eliminating the latter from the measurement the number of particle images crossing the ends of the array is greatly reduced and the accuracy of the measurement correspondingly increased. This measure has little effect on the linearity of the instrument (figure 13) but greatly improves the angle response, illustrated in figure 17 for ω_c=5.65. The response to variations in both pitch and yaw is closely cosinusiodal to $\pm 75°$ and r.m.s. variations remain small. The proportion of the measurement volume sensitive to each flow angle also remains fairly constant within these ranges. Other calculations show results at least this good for

$2.8 < \omega_c < 45$. Note that further improvements in angle response could be achieved by increasing the length of the outer rectangular elements and/or reducing the length of the central element. Also note that this type of device greatly improves the angle response when the cross-correlation timing scheme is used.

4. MEASUREMENTS

To examine the performance of the one-component DAV experimentally, measurements were made in attached and separated turbulent flows. Where possible comparisons were made with a hot-wire anemometer.

The flows were generated in a small blow-down open-circuit wind tunnel powered centrifugal fan (see Smith et al. (1990)). The tunnel has a rectangular test section 2.29m long and .235m wide. The last .330m of its length, where the measurements were made, is built entirely from plexiglas (figures 4 and 18). The height of the test section, which increases gradually along its length to maintain a zero streamwise pressure gradient, is about 114mm in the measurement section. Flow at the test section entrance consists of a uniform potential core surrounded by relatively thin boundary layers. By the measurement section, however, the boundary layers have grown, almost entirely engulfing the potential core. A moveable plate, placed over the blower entrance is used to control air speed. Potential core velocities of 10 and 20m/s were used in this study.

Measurements were made in the flow adjacent to the side test wall, shown in figure 4, along horizontal profiles at the mid height of the test section. Figures 4 and 18 show the coordinate system (X,Y,Z) to be used in presenting results; X is measured downstream from the wind tunnel exit, Y inwards from the test wall and Z completes a right-handed system. A pitot-static probe, located at X=-343mm, was used to monitor velocity in the potential core during both hot-wire and DAV measurements.

Hot-wire measurements were made using a TSI type 1210 T1.5 single sensor probe. This was held by a long sting attached to a computer controlled traverse gear located about 1m downstream of the test-section exit, outside of its jet. The probe stem was bent toward the test wall at an angle of about 15° to the X axis to enable measurements to be made very close to that surface. This arrangement produced less flow interference than if the probe were introduced through a test section wall. For all measurements the sensor was parallel to the Z direction, i.e. normal to the local mean flow direction and velocity gradient. The absolute position of the sensor was found by placing it as close as possible to the test wall and then using a cathetometer to measure the distance between the hot-wire prongs and their reflection in the wall, the overall accuracy being better than $\pm$.1mm. For the attached flows this uncertainty was further reduced by comparison of the mean-velocity measurements with a theoretical sublayer profile. This comparison led to a Y-datum adjustment of -.06mm in both flows, an error attributed to backlash in the traverse gear.

The hot wire was operated at an overheat ratio of 1.7 using a Dantec type 56C01 and 56C17 constant temperature bridge and main unit, balanced to give a frequency response of over 30kHz. The bridge output was read through an Analogic HS-DAS 12 A/D converter into an IBM AT computer where it was linearized. The hot-wire was calibrated by placing it in the potential core next to the reference pitot static and varying the flow speed. Flow temperature was monitored during calibrations and measurements. Temperature variations, $\pm$2°F at most, were corrected for using the method of Bearman

(1971).

For measurements with the DAV, 2.1μ polylatex spheres were introduced to the flow through a jet-type atomizer placed at the blower outlet. The spheres were suspended in alcohol which evaporated soon after their injection into the flow, resulting in a monodisperse distribution of particle sizes. To enable DAV measurements close to the test wall the laser beam was introduced at a slight angle (0.6°) to the Z-axis (see figure 4). Its diameter in the measurement volume was adjusted to 0.4mm at the $1/e^2$ points using the collimator. Diameter in the measurement volume was estimated by measuring the beam diameter and convergence angle at the collimator output and the optical path length. Judging from the shapes of the DAV signals, a smoother, more Gaussian intensity distribution was achieved if the beam was brought to its focus before, rather than after, the measurement volume. The Y position of the DAV measurement volume was measured to an accuracy of $\pm$.02mm using a dial indicator mounted between the outside of the test wall and optical table. The dial indicator was set to zero with the center of the measurement volume at the wall. This position was found by monitoring the d.c. output of the photo-diode amplifiers. Near Y = 0 the laser beam strikes the wall at a glancing angle and light is scattered from the surface. When the measurement volume intersects the wall this scattered light is received by the photodiode elements. When the center of the volume is at the wall the light received by the elements is at a maximum. By maximizing the d.c. output of the photodiode amplifiers the measurement volume center could be placed at the wall to an accuracy of better than $\pm$.1mm. For the attached flows

this uncertainty was further reduced by comparison of the mean-velocity measurements with a theoretical sublayer profile. This comparison led to an Y-datum adjustment of +.04mm in both flows, the consistency of this error suggesting some bias in the above positioning scheme. Note that in contrast to LDA scattered light from the wall is not a problem in making near-wall measurements since it merely adds a d.c. level to the signals.

At most measurement locations typically 400 measureable signals per second were visible in the DAV outputs, this rate being consistent with seeding density and measurement volume dimensions. Signals were analyzed using the cross-correlation timing scheme. Cross-correlations were performed by reading them into an IBM AT computer using a Rapid Systems R2000 A/D converter, the A/D inputs being buffered with two x10 buck and gain amplifiers. The R2000 is an 8-bit 2 channel A/D converter with a peak sampling frequency of 20MHz per channel. The external trigger of the R2000 A/D converter was used detect the presence of a signal by monitoring one of the outputs, its threshold being set just above the noise level. Since pre-trigger samples were taken the same output could be used to trigger data acquisition regardless of the flow direction. At most locations, 192 pretrigger and 320 post-trigger samples were taken simultaneously on both channels, the sampling rate being adjusted between 20Mhz and 500kHz according to local flow conditions. Cross-correlations were performed with the aid of an 18-8 Laboratories PL2500 array processor. As in the simulation a 7-point least-squares parabola was used to interpolate the position of the peak. To allow further study of the

DAV characteristics, signals were also stored on optical disc (a procedure that would not normally be necessary). Writing to disc was a relatively slow process and reducing the data rate to about 15 per second. Between 1000 and 4000 DAV signals were processed at each measurement point. Statistics were calculated using particle averages.

4.1 Attached flows

Measurements were made in the undisturbed test wall boundary layer at x=-165mm for edge velocities of 10 and 20 m/s. Figures 19a-d compare hot-wire and DAV measurements of mean velocity U/U_e, turbulence normal stress $\overline{u^2}/U_e^2$ and skewness factor $\overline{u^3}/(\overline{u^2})^{1.5}$ for the 10m/s flow. The agreement between the mean velocity measurements (figures 19a and b) appears very good. The largest difference, of about $2.5\%U_e$, occurs in the buffer layer (figure 19b) where the hot-wire measurements lie slightly below those of the DAV. Figure 19b appears to show the DAV capable of useful mean velocity measurements as close as .2mm from the wall, within the sublayer. This limit is consistent with the 0.4mm diameter of the laser beam in the measurement volume.

Agreement between the turbulence stress measurements at 10m/s is also satisfactory except within the near-wall region ($y < 0.8$mm) and close to the outer edge of the boundary layer ($y > 40$mm), see figure 19c. The discrepancies in the near-wall region are almost certainly caused by velocity gradient broadening of the DAV measurement, i.e. an additional apparent turbulence stress due to significant variations

in mean velocity across the measurement volume. This error is well documented for LDA applications (see for example Durst et al. (1981)). To first order the additional turbulence stress is given by $(\Delta\partial U/\partial Y)^2$ where Δ is a distance representing the standard deviation of the distribution with Y of particles passing through the measurement volume. Based on the dimensions and form of the DAV measurement volume we would expect this distance to be of the order of 0.1mm. In fact, setting Δ=0.075mm corrects well for the difference between the hot-wire and DAV results, as evidenced in figure 20a. The differences in the normal stress measurements in the outer region are due to electrical noise in the DAV. At the furthermost point from the wall (y=91mm) this adds about $0.001U_e^2$ to the normal stress. As is evidenced by figure 19c and predicted by equation 4 this error is not constant across the boundary layer but decreases as the fourth power of the mean velocity. It is important to note that this lower limit on normal stress measurements, due to electrical noise, is not a fundamental one. Increasing laser power, moving to a more advantageous receiving angle, using a smaller laser beam and greater receiving lens magnification are all measures that would reduce $\overline{t_n^2}$.

As with the normal stress, agreement between the measurements of skewness factor (figure 19d) is best in the mid region of the boundary layer. Close to the wall (Y < 1mm) the DAV consistently underestimates skewness by about 0.2. In the very near-wall region (Y < .5mm) this appears to be due to velocity gradient broadening of the normal stress, since here correcting the normal stress using Δ=.075mm brings the two

measurements into closer agreement (figure 20b). The remaining discrepancy may be partly due to second-order broadening, i.e. curvature of the mean profile within the volume. This error, which would tend make the skewness more negative, would be greatest in the buffer layer, much like the differences observed here.

The mean-velocity measurements made with an edge velocity of 20m/s (figures 21a and b) agree almost as well as those at the lower speed. Again the greatest discrepancy between hot-wire and DAV (about 3.5%U_e) occurs in the buffer layer. As at 10 m/s the turbulence normal stresses (figure 21c) are in close agreement except in the near wall region and towards the boundary layer edge. Again velocity gradient broadening appears responsible for the near-wall errors, corrections with $\Delta = .075$mm eliminating most of the differences here (figure 22a). Errors in the edge region resulting from electrical noise are actually less severe than at 10m/s bearing in mind that, scaled on U_e, equation 4 predicts an increase of 4 times in the normalized turbulent stress error with a doubling of the mean velocity. The apparent change in $\overline{t_n^2}$ between the two profiles reflects the fact that this parameter is quite sensitive to optical alignment of the DAV system, which was adjusted between these measurements. Alignment of the axis of the photodiode array with the laser beam center and focussing of the receiving lens were found to be particularly important in this respect. The skewness profile comparison (figure 21d) is similar to that at 10m/s except that the disagreements close to the wall ($Y < 2$mm) are more severe. Applying gradient broadening corrections to the normal stress reduces differences very

near the wall (figure 22b) but, as at 10m/s does not improve agreement in the buffer region.

4.2 Separated flow

The satisfactory performance of the DAV in the attached flows, while gratifying, could have been predicted from its theoretical angle response curves. At the relatively small instantaneous flow angles experienced in a turbulent boundary layer these are closely cosinusiodal. In a separated flow, however, instantaneous flow angles reach 90°. Errors due to the imperfections in angle response would therefore be expected. Observing these errors was only a one reason for performing separated-flow measurements. The primary purpose was to uncover any other unforeseen problems that would limit the performance of a DAVs with better photodiode array designs.

A separated flow was generated in the measurement section by placing a fence on the test wall at X=-267mm. The fence, shown in figure 18, had a rectangular cross section 12.7mm high by 6.4mm thick and completely spanned the test wall. It generated a region of recirculating flow roughly 150mm in length.

The DAV was used to measure three profiles in this flow at X = -117mm, -165mm and -213mm for an approach edge velocity U_e of 10m/s. Hot-wire measurements were made only at X = -165mm in the region outside the separation where local turbulence levels were less than 30%. Because of the high turbulence intensities and instantaneous flow reversals in these flows the particle averaging used to determine

statistics from the DAV measurements was expected to produce some bias error. This type of error has been well researched for LDA applications (see for example Fuchs et al. (1992)) and was corrected, as it usually is for LDA measurements, by weighting each velocity sample by the measurement volume transit time of the particle that produced it.

Figures 23 through 25 show mean velocity, turbulence normal stress and forward flow fraction[2] profiles. Broadly speaking these measurements are consistent with the results of previous recirculating-flow studies (see for example Moss et al. (1980), Eaton and Johnston (1980), Devenport and Sutton (1993)). Qualitatively, at least, they demonstrate the ability of the DAV to make useful measurements in a reversing flow.

The mean profiles (figure 23a) show the steep velocity gradient associated with the separated shear layer and its relaxation with distance downstream. They also show the mean backflow which has a peak magnitude of $-0.24U_e$ at X = -213mm (4.27 fence heights H from separation) and $-0.21U_e$ at X = -165mm (8.06 H from separation). The profile at X = -117mm appears to be measured close to the reattachment location. Also visible at X = -165mm and -213mm are the 'sub-boundary layers' formed underneath the backflow. A close examination of the near-wall sections of these profiles (figure 23b) shows them to be consistent with the no-slip condition down to about .2mm from the wall. This lower limit on Y is in agreement with the attached flow results.

The profiles of turbulence normal stress and forward flow fraction (figures 24 and

[2]Fraction of time for which the flow is in the positive X direction.

25) also show the separated shear layer. At X = -213mm and -165mm the peak turbulence normal stress is $0.057U_e^2$ (23.9% turbulence intensity). By X = -117mm it has dropped to $0.035U_e^2$ (18.7%). Agreement with the hot-wire measurements made in the outer part of the shear layer at X = -165mm appears satisfactory.

Without quantitative comparisons the limitations of the DAV angle response are not visible in the above measurements. They are visible, however, in velocity histograms. Figure 26 shows a selection of histograms from the profile at X = -165mm. At all locations where instantaneous flow reversals occur the histograms have a 'hole' in the vicinity of zero velocity. While this is almost certainly . consequence of the imperfect angle response it appears also to be due to the limited duration of the signals recorded by the A/D converter with each particle transit. The finite record duration limits the maximum measurable transit time and thus the minimum velocity magnitude. The effects of increasing the duration can be seen by comparing the histograms measured at Y = 10.2mm and 7.6mm, for example, and noting the difference in $\overline{u'^2}/U_e^2$ at these locations (figure 24). Between these points the duration was doubled by halving the sampling rate, resulting in a corresponding reduction in the size of the hole. In general, however, reducing the sampling rate may not be the best way of controlling this phenomenon since it degrades the resolution of the DAV for small transit times (i.e. high velocities), forcing a heavy reliance on the scheme used to interpolate the cross correlation function. In most separated flows, as in this one, there are points where both high velocities and near-zero

velocities occur. A more satisfactory solution is to increase the record duration by increasing the number of samples. This would be a simple matter with the present equipment since the R2000 can take up to 132,000 samples in each record. An alternative, if this capability were not available, would be to count the number of records for which signals are detected on one channel but not the other and then assign these samples a velocity of zero. This type of scheme has been successfully implemented with pulsed wire anemometers (Bradbury and Castro (1971)).

In summary, the separated flow measurements revealed no fundamental problems that could limit the accuracy of improved DAV designs.

5. CONCLUSIONS AND FUTURE WORK

A new flow measurement technique, the diode array velocimeter, has been proposed. A DAV works by timing the passage of seed particles through a small section of a light beam. This is achieved by imaging light scattered by the particles on to one or more photodiode arrays. The arrays have a few carefully shaped elements, the shape and position of the elements being used to control the measurement volume geometry and thus select the measurement made. Measurement volumes sensitive to velocity, position and acceleration may be designed.

A DAV for one-component velocity measurements has been developed to demonstrate this concept. This device uses a single photodiode array with two long rectangular elements placed side by side (figure 2). A 0.4-mm diameter laser beam is used to illuminate seed particles in a fluid flow. Light scattered by the particles at 90° to the beam is collected by a lens and focussed on to the array, resulting in a measurement volume consisting of two parallel 'plates' (figure 3). The time between a particle image being detected by the photodiode elements gives the velocity component normal to the long axis of the array. The direction of the velocity is given by the order of detection. Two different methods for determining the transit time were investigated. The first method involves cross-correlating the signals and then measuring the time delay of the peak correlation coefficient. The second method involves comparing the signals to a trigger level set just above the noise. The time at which each signal crosses the trigger

level is recorded. The time difference is then taken as the transit time.

A theoretical analysis has been performed to examine the influence of electrical noise on the measured velocity. Noise produces an apparent additional turbulence normal stress, the magnitude of which (when normalized on mean velocity) increases as the mean-velocity squared. However, the magnitude drops if the optical magnification of the receiving lens is increased, allowing the laser beam to be focussed. Maximizing the magnification has the added benefit of minimizing the measurement volume size. The optical magnification of the present receiving lens was 10, resulting in a measurement volume 0.104mm wide (D), 0.457mm long (h), and 0.4mm deep, the latter dimension being the diameter of the laser beam (4 times its r.m.s. width σ).

The angle response of the DAV was examined by simulating the signals generated by the photodiode elements for a range of conditions. For the cross-correlation timing scheme, the yaw and pitch response were found to be closely cosinusoidal to angles greater than 60° as long as signals producing peak correlation coefficients less than 0.95 were ignored. These limitations are largely a function of photodiode design. Even if the design is restricted to two rectangular elements, the response can be substantially improved by increasing the aspect ratio of the array h/D and reducing the measurement volume to beam size ratio D/σ. For the trigger timing scheme the pitch and yaw response are much poorer and variations in angle response with position in the measurement volume are large. Eliminating signals smaller than a certain peak magnitude substantially improves the pitch response, but the yaw response remains poor. We therefore conclude

that, for this particular photodiode array design, triggering cannot produce accurate velocity measurements in most flows. Altering the array design to include a third central element, however, can produce a measurement volume with very satisfactory pitch and yaw response when the trigger timing scheme is used.

Measurements were performed in two attached boundary layer flows (edge velocity 10 and 20m/s) and in a separated flow formed behind a fence (edge velocity 10m/s) using the cross-correlation timing scheme.

In the boundary-layer flows detailed comparisons were made with hot-wire measurements. In both flows DAV and hot-wire mean velocities agree well. The DAV appears capable of mean velocity measurements down to about .2mm from the wall. Normal stress and skewness profiles are also in good agreement, except in the near-wall and edge regions. Satisfactory agreement is obtained in the near wall region after correcting for velocity gradient broadening. Discrepancies in the edge region are a consequence of electrical noise which produced an apparent additional stress of about $0.001 U_e^2$.

Measurements made with the fence demonstrate the ability of the DAV to make useful measurements in turbulent reversing flows. All expected features of the separated shear layer and recirculation are observed including the sub-boundary layer formed beneath the backflow. Histograms measured in the reversing part of this flow show a hole near zero velocity that is a consequence of the imperfections in the DAV angle response and the limited duration of the photodiode signals correlated to determine the transit time.

Neither of these problems is fundamental. Using a better photodiode array design and increasing the duration of the photodiode signals used in the cross-correlation should eliminate or, at least, greatly reduce this effect.

We have already described some design changes that would improve the 2-element photodiode array for one-component velocity measurements and so ne simplifications in its transit time determination scheme. In future work we also hope to switch from PIN to avalanche photodiode arrays (APDs). In most circumstances APDs produce less noise and have a much better frequency response so, given equation 10, would be expected to greatly improve DAV performance.

A potentially useful technique in DAV design we are considering is to optically overlay different photodiode arrays. This is achieved by splitting the light focused by the receiving lens and examining the same part of the image with differe:: detectors. This technique could be used, for example, to improve the angle response of the present photodiode array by overlaying a small circular element at its center (figure 27a). Only particle images crossing that element would be measured. This would have the added benefit of greatly reducing the effective measurement volume size in the y and z directions. Overlaying three detectors in this way (figure 27b) could be a relatively simple way of making simultaneous two component velocity measurements from one receiver angle.

Finally we anticipate a range of new photodiode arrays designed for different purposes and the use of more than one receiving angle for two or three component

measurements. Examples of possible array designs are given in figures 27c and d. Figure 27c shows a one-component velocity and position sensing array - the inner two elements are used to sense velocity, the outer two the y-location of the particle image. Accuracy of velocity measurements could be improved by making a sequence of two or more measurements on the same particle as implied by the design in figure 27d. Such a device, at least in principle, could also measure particle acceleration.

ACKNOWLEDGEMENTS

The authors gratefully acknowledge the support of the Office of Naval Research, under grant number N00014-92-J-1292 and of their technical monitor, Mr. James A. Fein. We would also like to thank Mr Ken Wittmer and Mr. Michael Rife for their assistance with the hot-wire measurements and Dr. Roger Simpson for his helpful advice.

REFERENCES

Bearman P W, 1971, "Corrections for the effect of ambient temperature drift on hot-wire measurements in incompressible flow", DISA Information, vol. 11, pp 25-30.

Bradbury L J S and Castro I P, 1971, "A pulsed-wire technique for velocity measurements in highly turbulent flows", Journal of Fluid Mechanics, vol. 49, pp. 657-691.

Boutier A and Lefevre J, 1988, "Mosaic laser velocimeter", 4th Symposium on Applications of Laser Anemometry to Fluid Mechanics, Lisbon, Portugal.

Devenport W J and Sutton E P, 1993, "An experimental study of two flows through an axisymmetric sudden expansion", Experiments in Fluids, in press.

Durst F, Melling A and Whitelaw J H, 1981, Principles and Practice of Laser Anemometry, Academic Press.

Eaton J K and Johnston J P, 1980, "Turbulent flow reattachment:- an experimental study of the flow and structure behind a backward-facing step", Dept. of Mech. Eng., Stanford University, Rept. MD-39.

Fuchs W, Albrecht H, Nobach H, Tropea C and Graham L J W, 1992, " Simulation and experimental verification of statistical bias in laser Doppler anemometry including non-homogeneous particle density", 6th Symposium on Applications of Laser Anemometry to Fluid Mechanics, Lisbon, Portugal.

Hirleman E D, Yue Y, Berman N S, Guan D X, 1984, "Single laser beam velocimetry

(L1V) in turbulent flows", 2nd Symposium on Applications of Laser Anemometry to Fluid Mechanics, Lisbon, Portugal.

Moss W D and Baker S , 1980, "Recirculating flows associated with two-dimensional steps", Aeronautical Quarterly, vol. 31, pp 151.

Ohmura K, Hishada K and Maeda M, 1992, "A mutli-angle laser-two-focus velocimeter using photodiode arrays", 6th Symposium on Applications of Laser Anemometry to Fluid Mechanics, Lisbon, Portugal.

E J Smith, M C Rife and W J Devenport, 1990, "Investigation of the small boundary-layer tunnel", Report VPI-AOE-177, AOE Dept., VPI&SU.

APPENDIX - DEPENDENCE OF t'_n

If the transit time is determined from the DAV output signals using a trigger scheme one would expect the r.m.s. of t'_n to vary approximately as the r.m.s. electrical noise level divided by the rate of change of voltage at the leading edge of the signal where the trigger is fired, i.e.

$$\sqrt{t'^2_n} \sim \frac{\sqrt{v^2_{noise}}}{\partial v/\partial t} \tag{17}$$

Assuming that the time taken for the particle image to cross the edge of each photodiode element is negligible, the rate of change of voltage is determined approximately by the step response of the amplifier. It therefore depends on the peak signal magnitude V_s and the angular cutoff frequency ω_c,

$$\partial v/\partial t \sim V_s \omega_c \tag{18}$$

and so,

$$\frac{\sqrt{t'^2_n}}{T} \sim \frac{1}{S\omega_c T} \tag{19}$$

where $S = V_s / \sqrt{\overline{t_n^2}}$.

Now consider the situation where the transit time is determined as the time delay of the peak cross-correlation $R_{xy}(\tau) = \overline{x(t)y(t+\tau)}$. Here x and y are used to denote the two DAV signals. Determining the peak in R_{xy} is the same as determining the zero-crossing point of its first derivative. $\sqrt{\overline{t_n^2}}$ will thus vary as the uncertainty due to noise in $\partial R_{xy}/\partial\tau$ divided by $\partial^2 R_{xy}/\partial\tau^2$. Now,

$$\frac{\partial R_{xy}}{\partial\tau} = \overline{x(t)\frac{\partial y(t+\tau)}{\partial\tau}} = \overline{x_s(t)\frac{\partial y_s(t+\tau)}{\partial\tau}} + \overline{x_n(t)\frac{\partial y_s(t+\tau)}{\partial\tau}} + \overline{x_s(t)\frac{\partial y_n(t+\tau)}{\partial\tau}} + \overline{x_n(t)\frac{\partial y_n(t+\tau)}{\partial\tau}} \quad (20)$$

where x_s and x_n, and y_s and y_n are used to denote the signal and noise components of x and y respectively. The last three terms of equation 20 express the uncertainty due to noise in $\partial R_{xy}/\partial\tau$. They are non-zero because only finite lengths of x and y are correlated. One would expect the third of these to be negligible for significant signal to noise ratios. The other two should scale as $\sqrt{\overline{v_{noise}^2}} V_s \omega_c$ since the electrical noise is governed by the same amplifier frequency response as the signal. The second derivative of the correlation is

$$\frac{\partial^2 R_{xy}}{\partial \tau^2} = \overline{x(t)\frac{\partial^2 y(t+\tau)}{\partial \tau^2}} \tag{21}$$

which should scale as $V_s^2 \omega_c^2$. Dividing these two results we once more obtain equation 19.

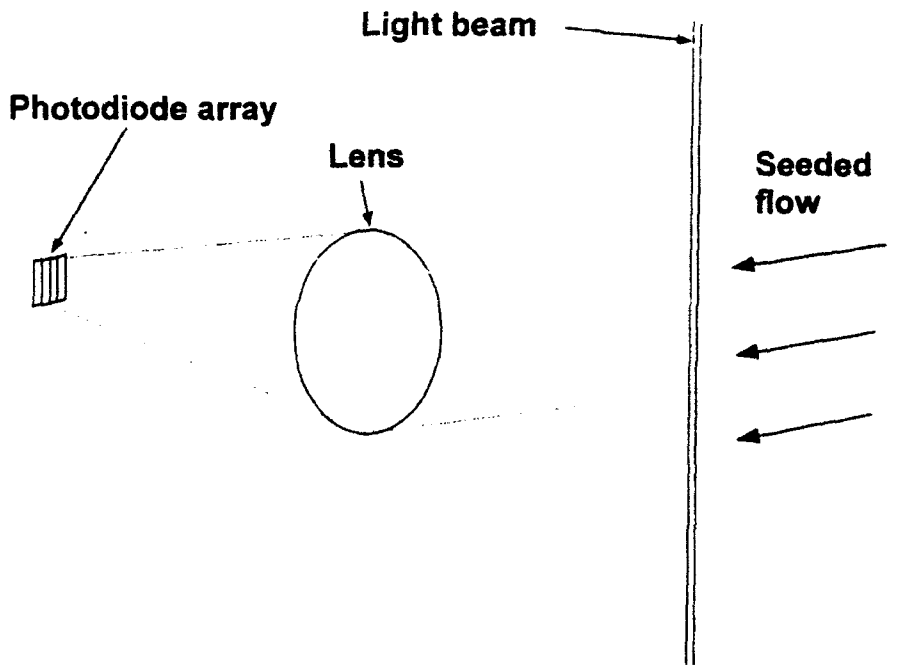

Figure 1. Simplest possible optical layout for a DAV.

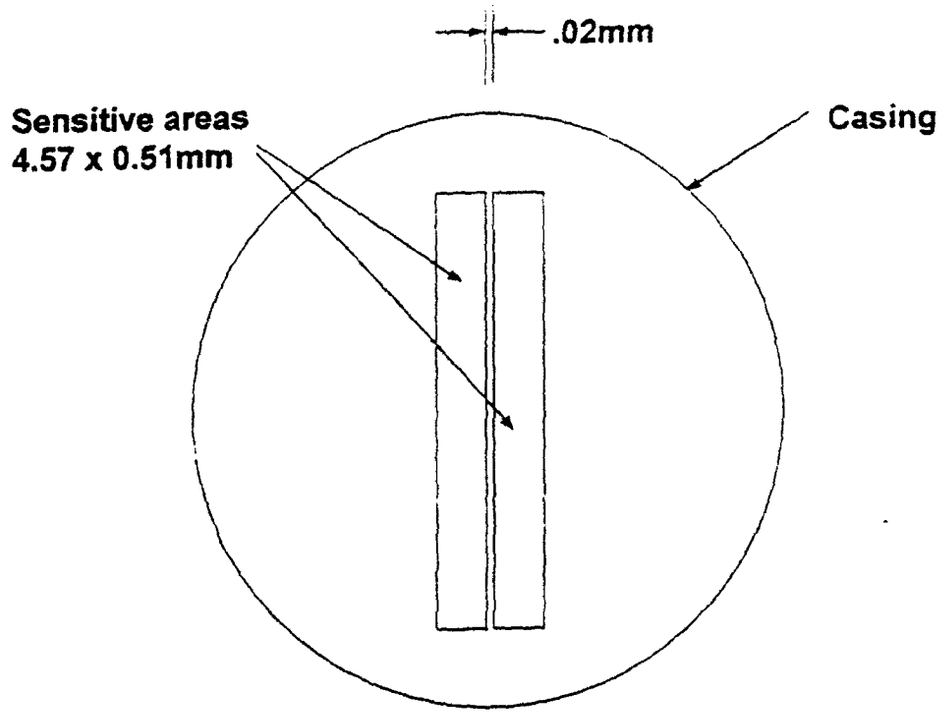

Figure 2. The Silicon Detector Corporation SD160 photodiode array.

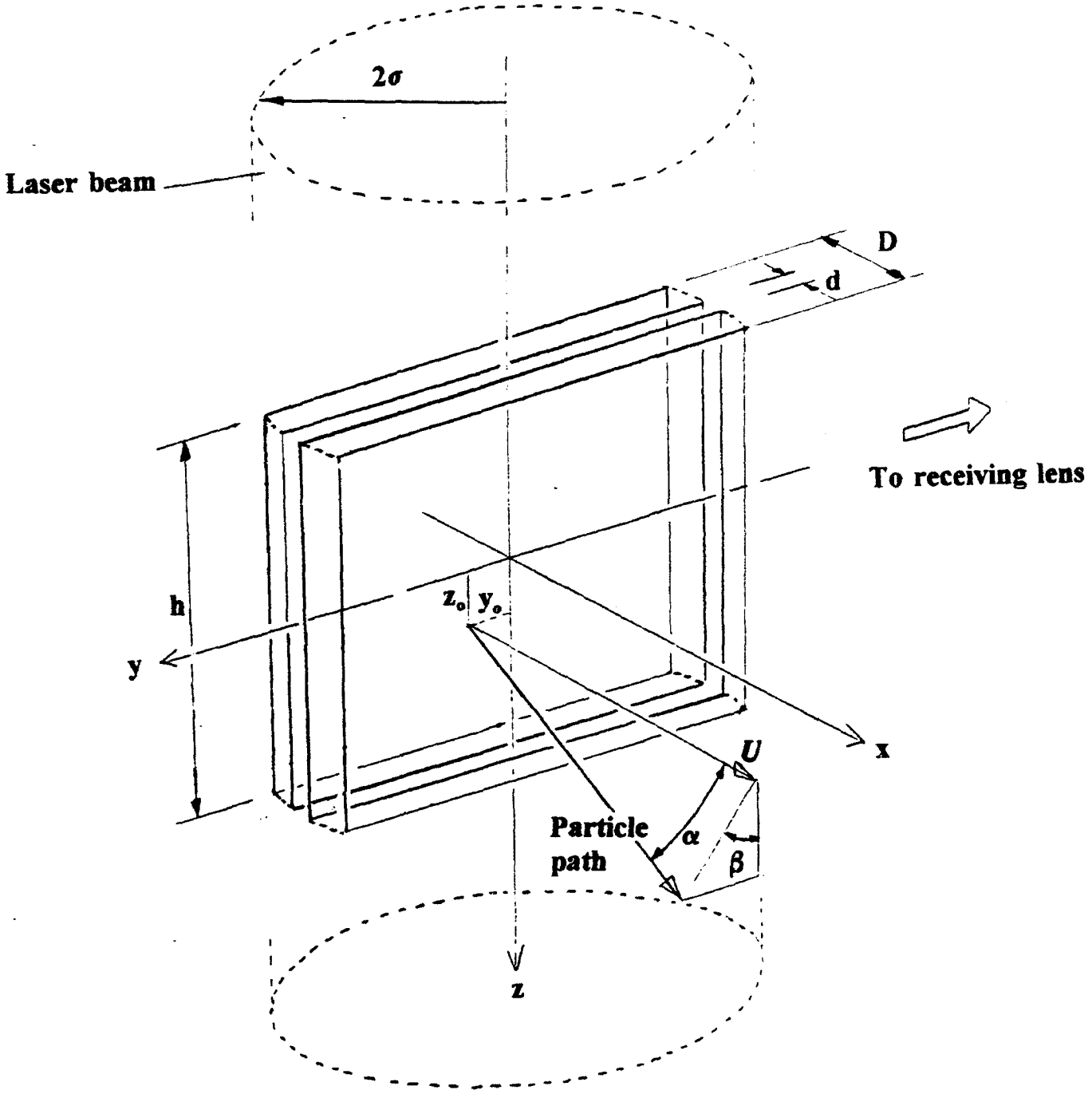

Figure 3. Measurement volume of the one-component DAV.

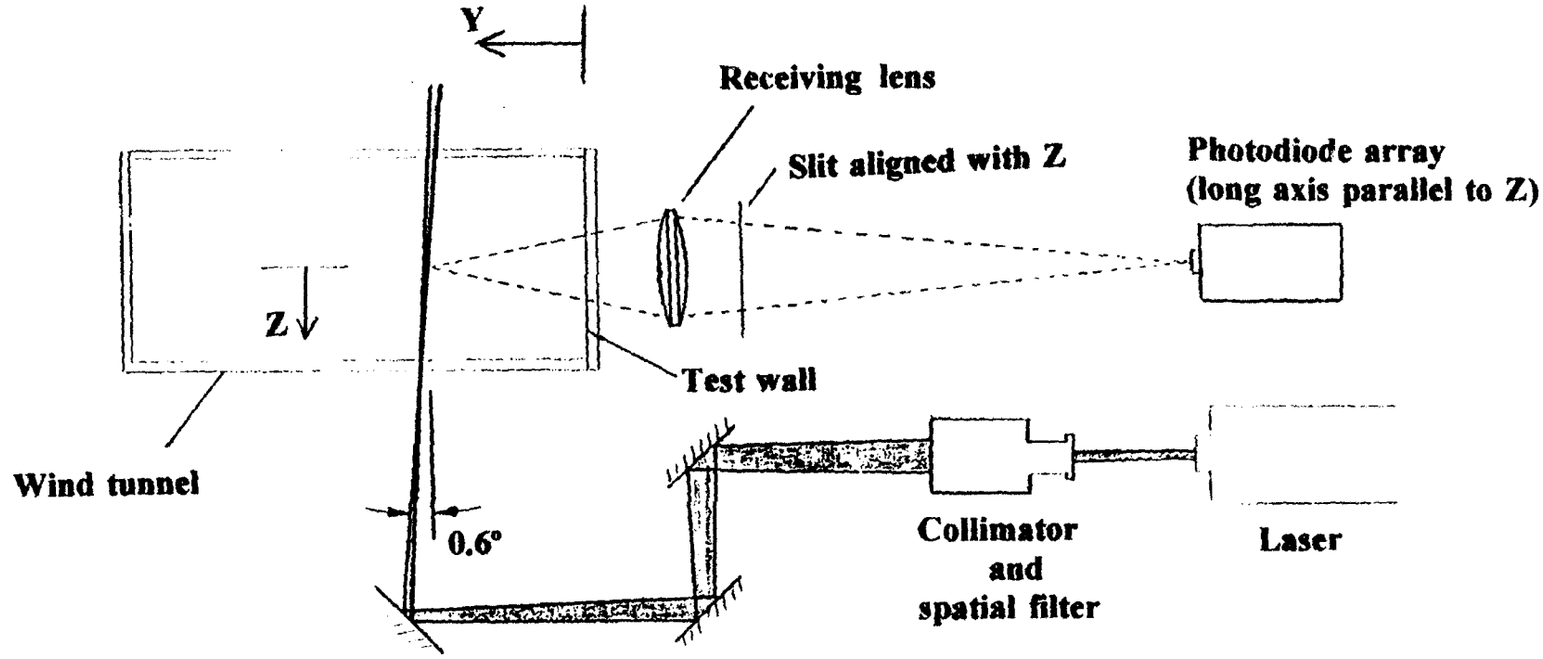

Figure 4. Schematic showing of the optical system and wind-tunnel cross section.

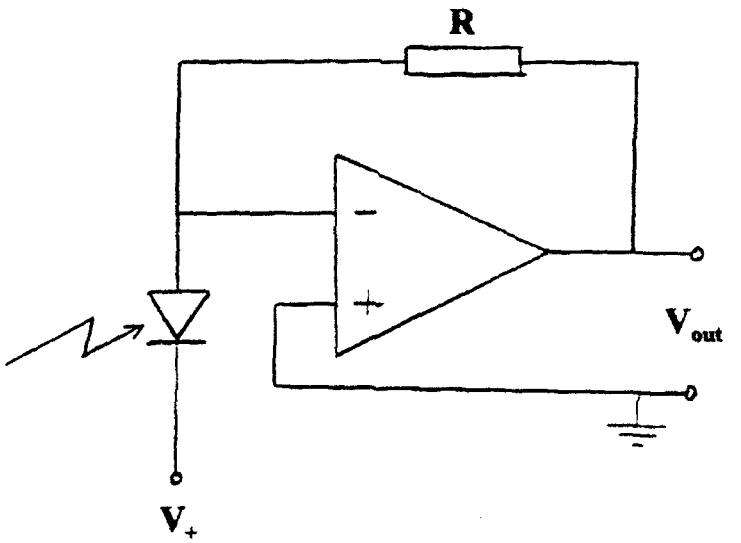

Figure 5. Circuit used to amplify current signals produced by photodiode element. $R = 7 \times 10^6 \Omega$. $V_+ = 15V$. Amplifier is a Burr-Brown OPA 627.

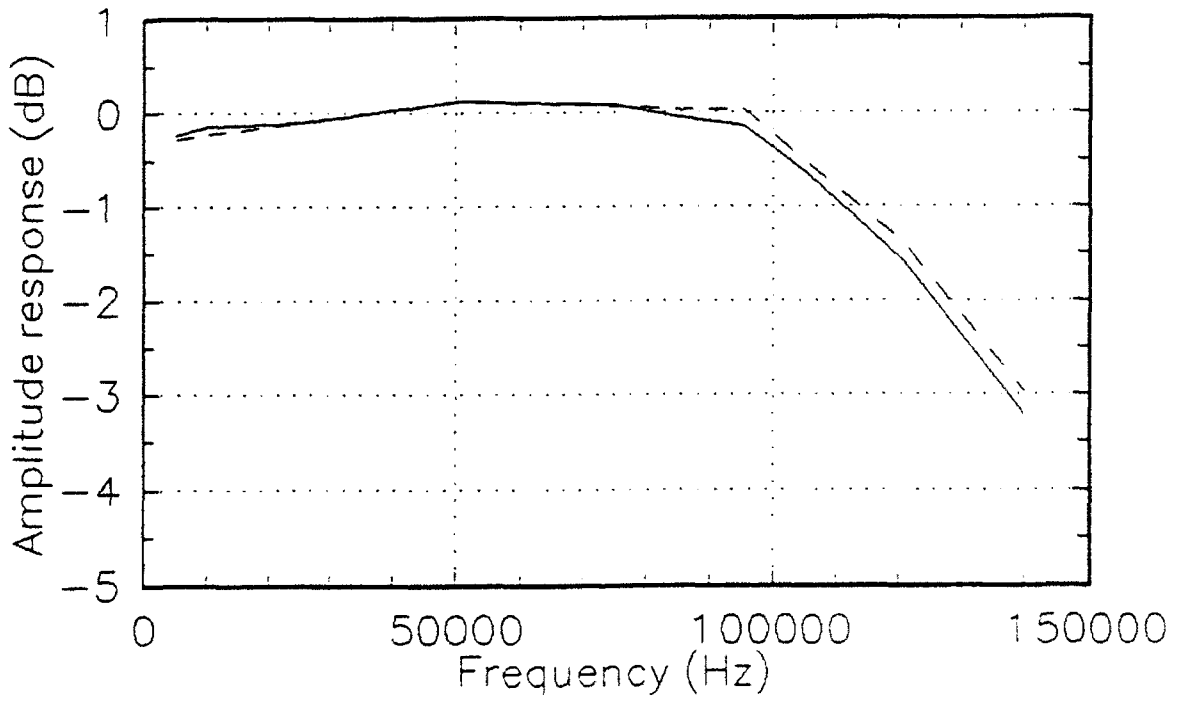

Figure 6. Frequency response curves for the photodiode elements and their amplifiers.

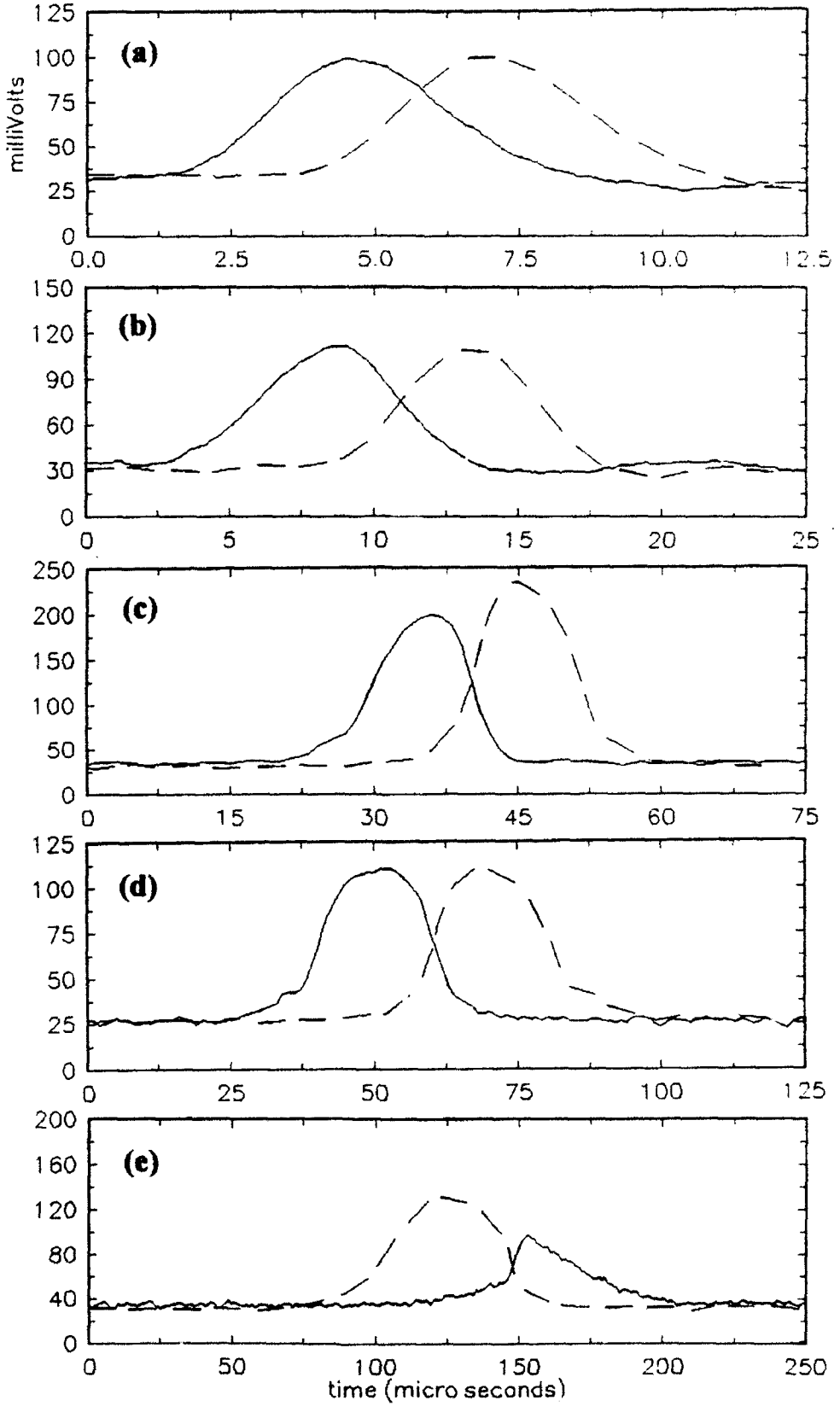

Figure 7. Typical DAV output signals, solid line - channel 1 (upstream), dashed line - channel 2 (downstream). (a) 20.6m/s (b) 9.9m/s (c) 4.5m/s (d) 2.4m/s (e) -1.4m/s.

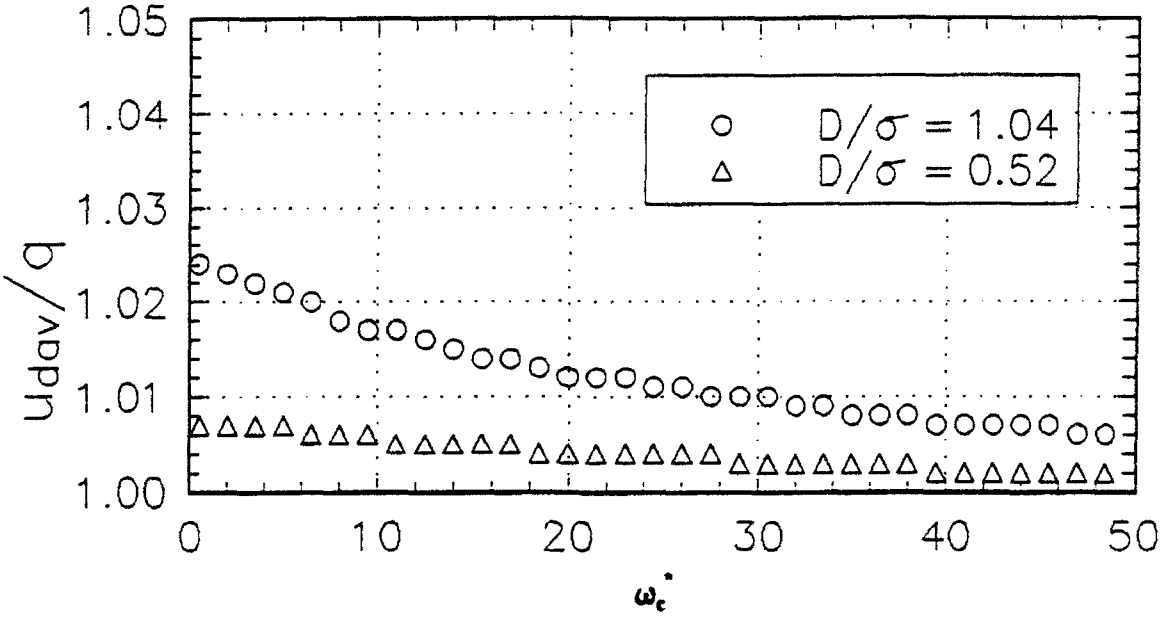

Figure 8. Velocity inferred from simulated DAV signals over actual velocity as a function of ω_c^* for zero pitch and yaw. For present system $D/\sigma = 1.04$.

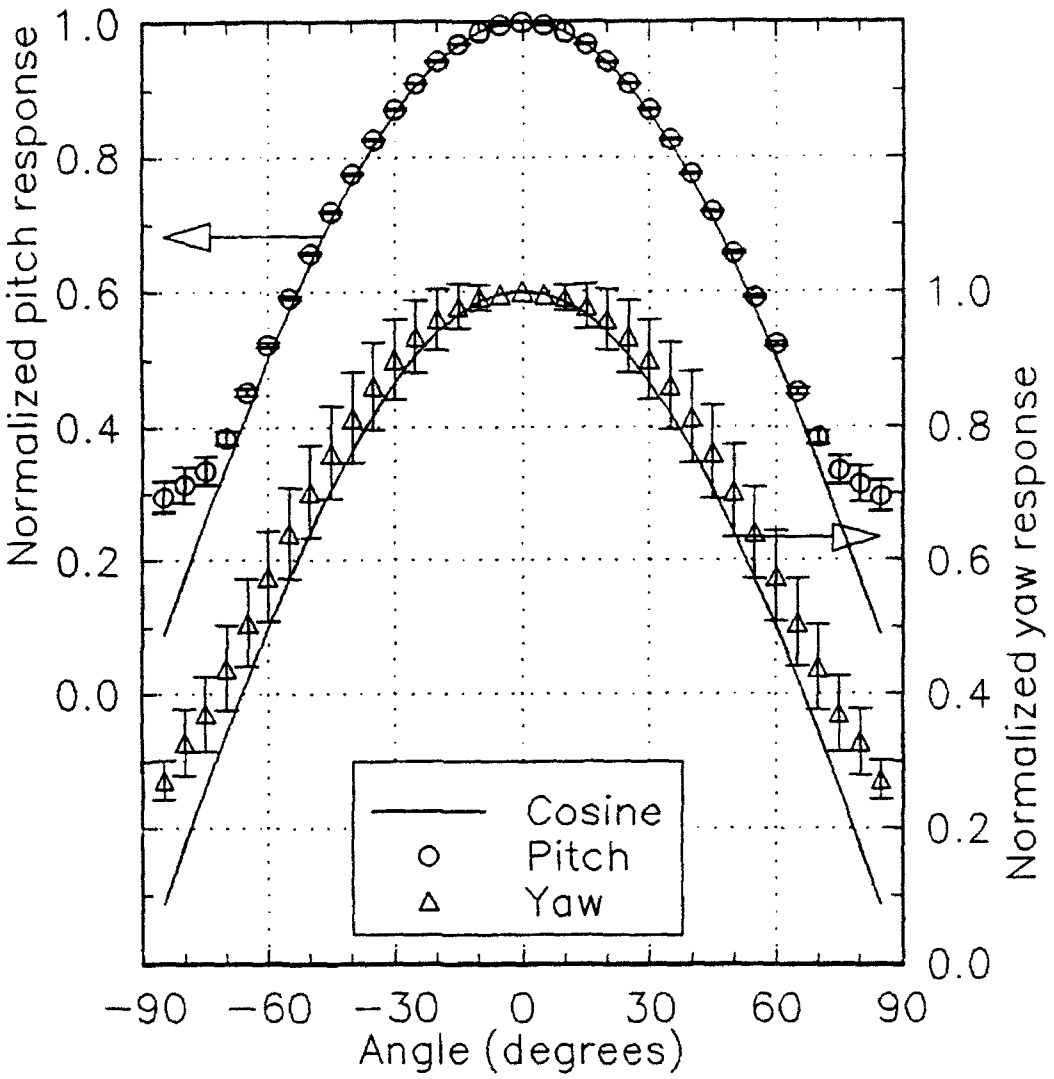

Figure 9. DAV angle response normalized on velocity at zero pitch and yaw, $\omega_c^* = 5.65$, no conditions on peak correlation coefficient. Points show average over measurement volume, error bars show r.m.s. variation.

(a)

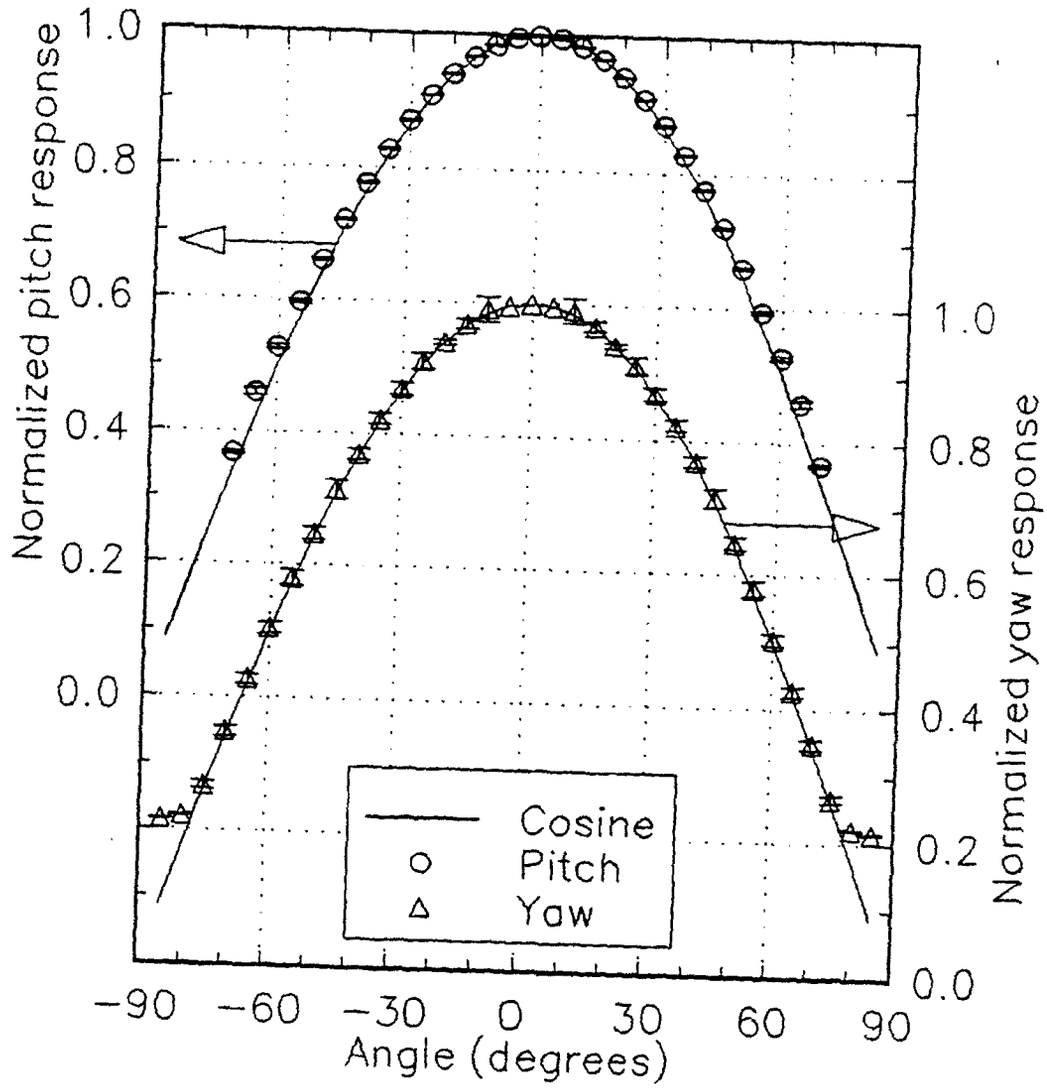

Figure 10. DAV angle response normalized on velocity at zero pitch and yaw for a minimum peak correlation coefficient of 0.95. Points show average over measurement volume, error bars show r.m.s. variation. (a) $\omega_c^* = 2.83$, (b) $\omega_c^* = 5.65$, (c) $\omega_c^* = 11.3$, (d) $\omega_c^* = 22.6$.

(b)

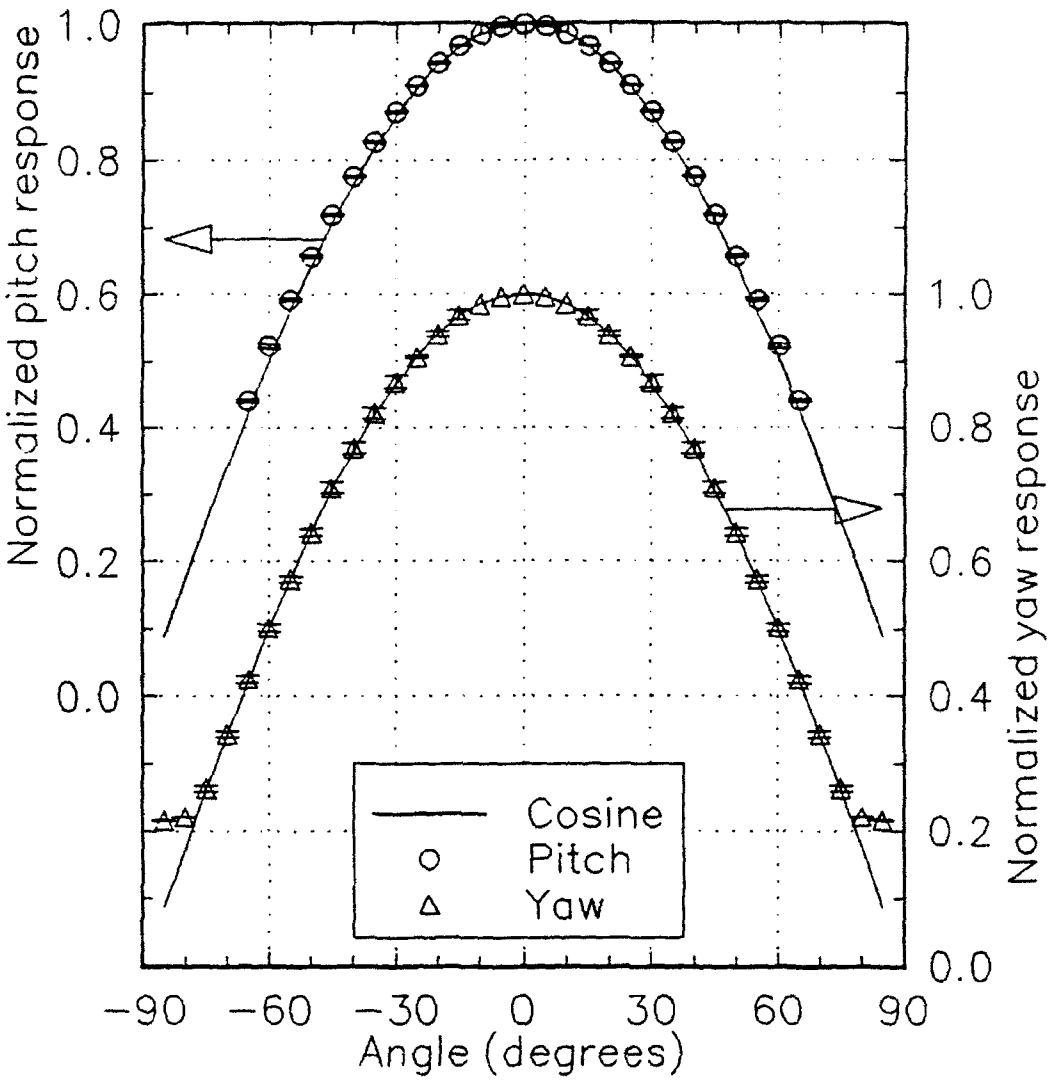

Figure 10. DAV angle response normalized on velocity at zero pitch and yaw for a minimum peak correlation coefficient of 0.95. Points show average over measurement volume, error bars show r.m.s. variation. (a) $\omega_c^* = 2.83$, (b) $\omega_c^* = 5.65$, (c) $\omega_c^* = 11.3$, (d) $\omega_c^* = 22.6$.

(c)

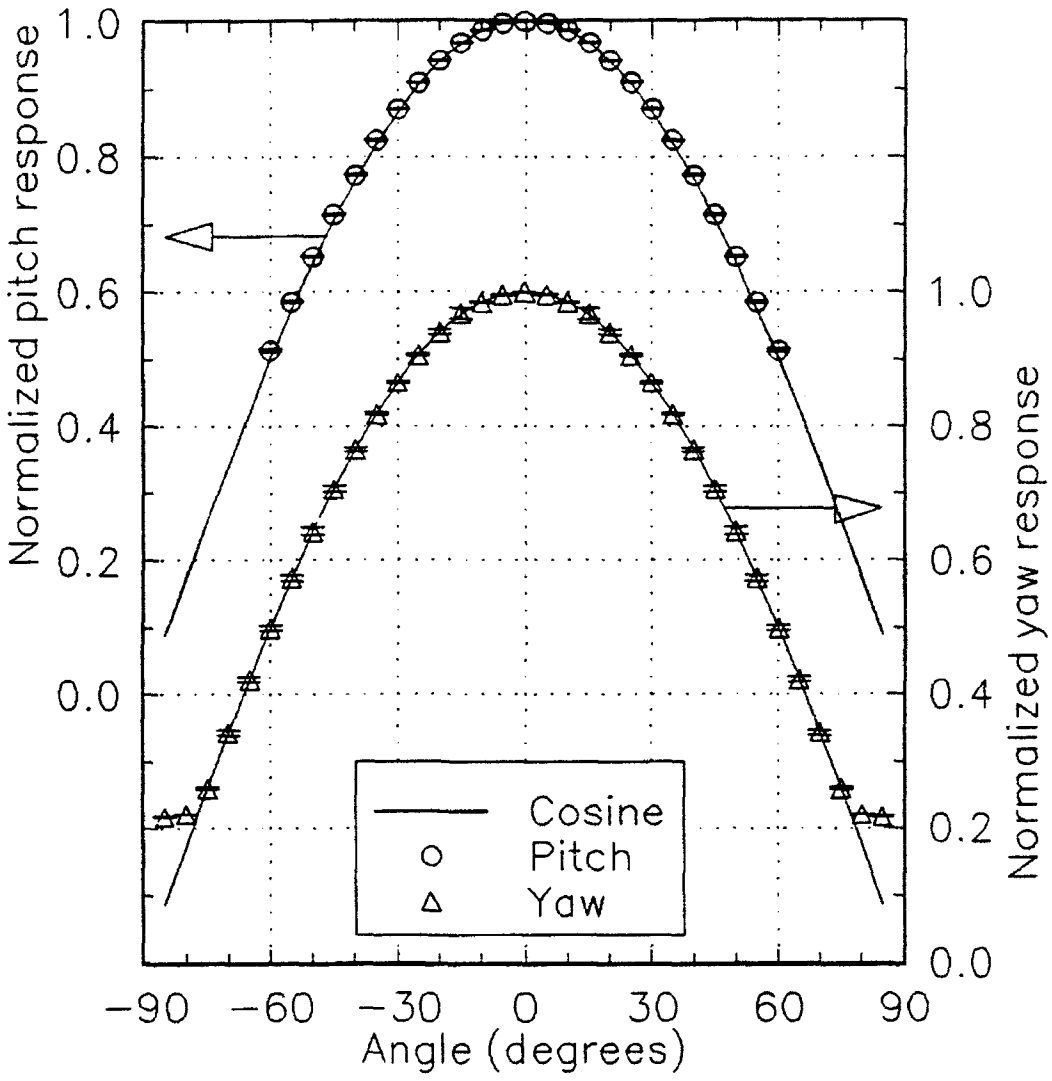

Figure 10. DAV angle response normalized on velocity at zero pitch and yaw for a minimum peak correlation coefficient of 0.95. Points show average over measurement volume, error bars show r.m.s. variation. (a) $\omega_c^* = 2.83$, (b) $\omega_c^* = 5.65$, (c) $\omega_c^* = 11.3$, (d) $\omega_c^* = 22.6$.

(d)

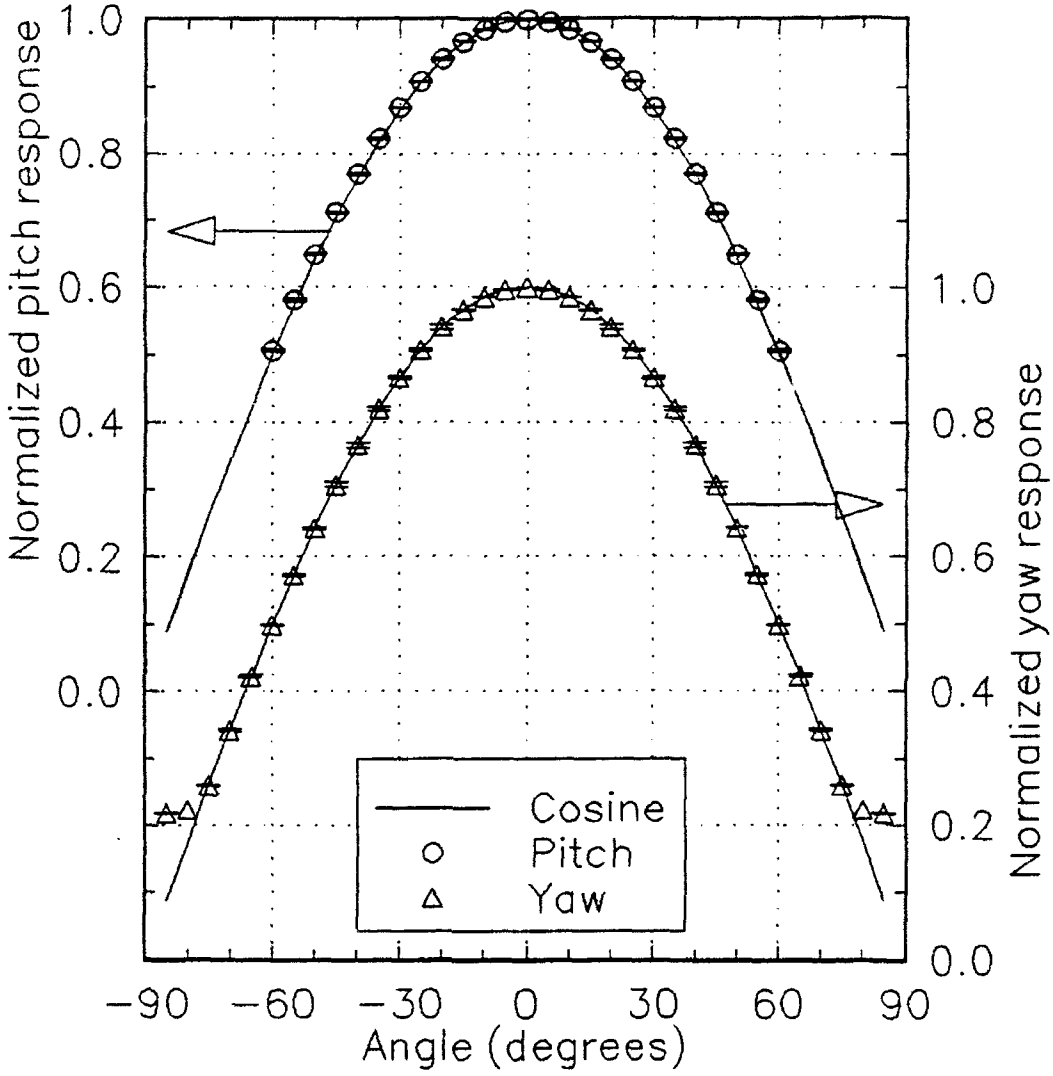

Figure 10. DAV angle response normalized on velocity at zero pitch and yaw for a minimum peak correlation coefficient of 0.95. Points show average over measurement volume, error bars show r.m.s. variation. (a) $\omega_c^* = 2.83$, (b) $\omega_c^* = 5.65$, (c) $\omega_c^* = 11.3$, (d) $\omega_c^* = 22.6$.

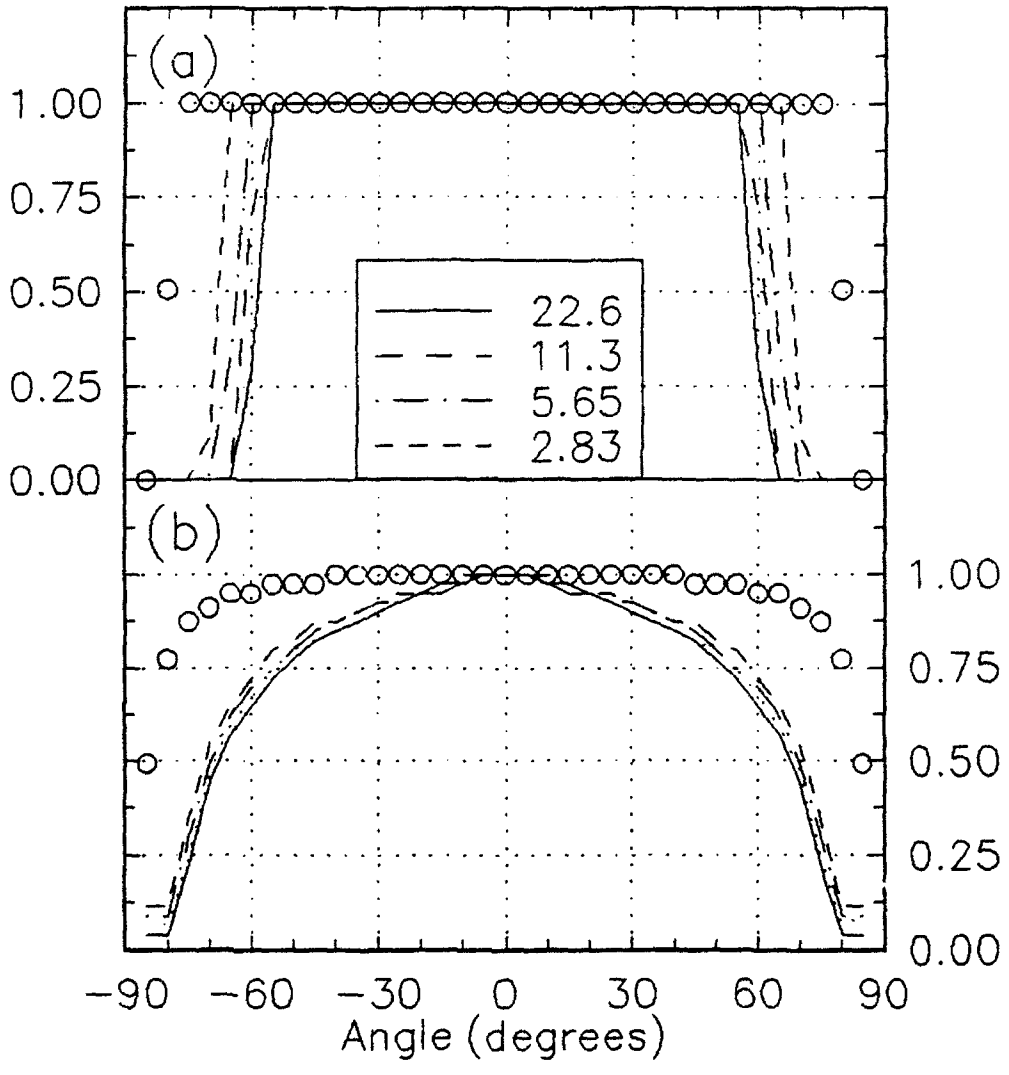

Figure 11. Proportion of the measurement volume sensitive to a particular flow angle for a minimum peak correlation coefficient of 0..95, (a) pitch (b) yaw. Legend shows values of ω_c^*. Points are for improved photo-diode array design with ω_c^* =5.65 and a minimum peak correlation coefficient of 0.9.

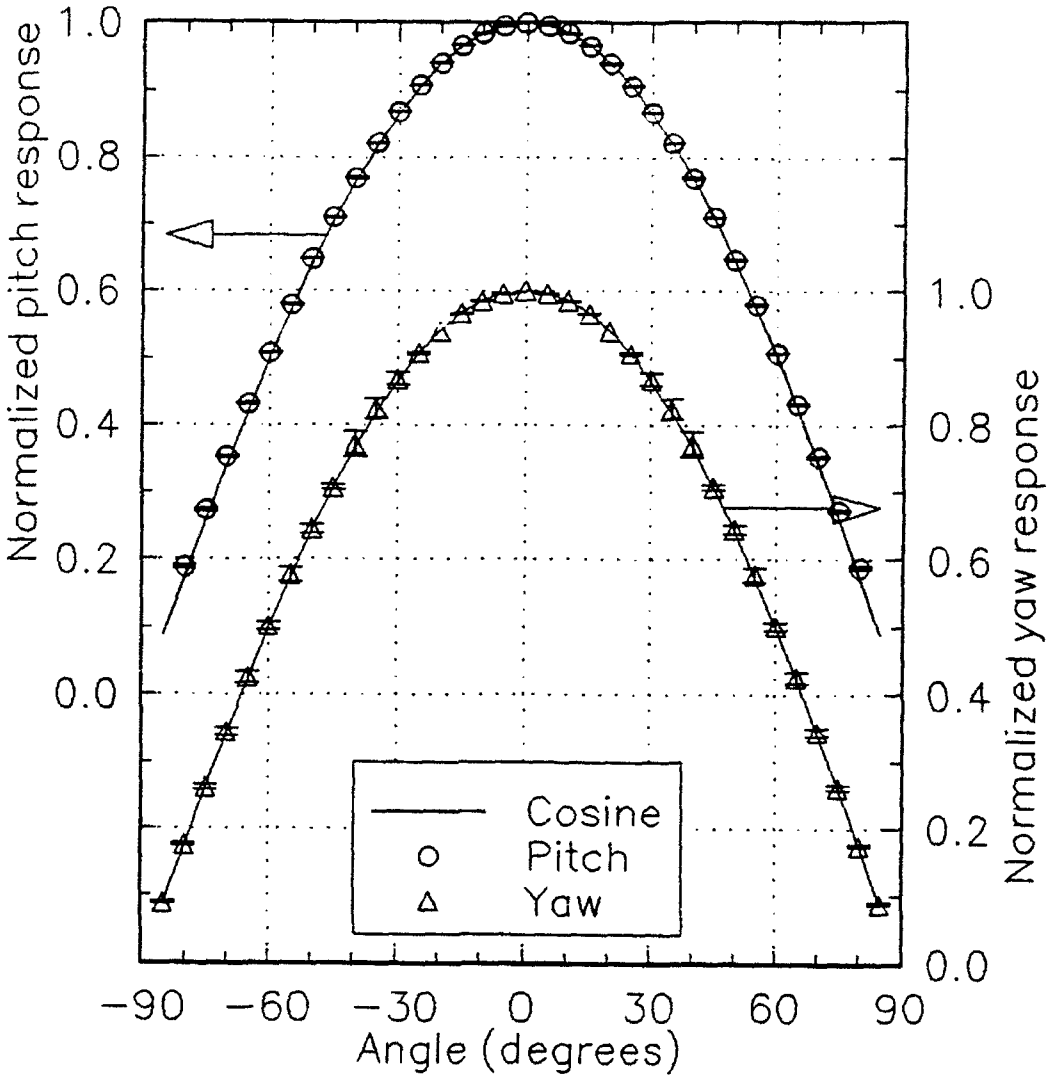

Figure 12. DAV angle response normalized on velocity at zero pitch and yaw for improved photodiode array design. $\omega_c^* = 5.65$, minimum peak correlation coefficient = 0.9. Points show average over measurement volume, error bars show r.m.s. variation.

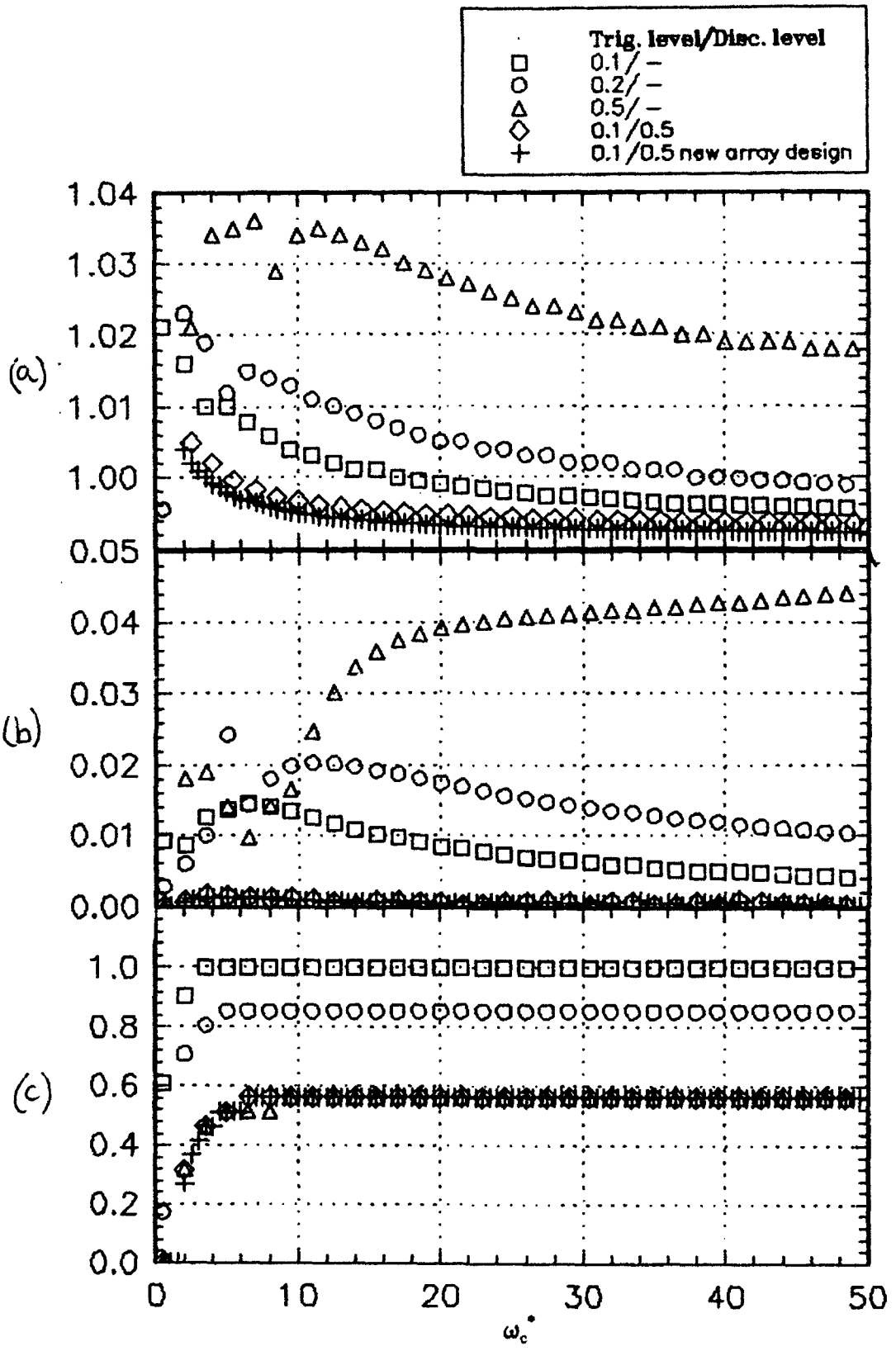

Figure 13. Velocity inferred from simulated DAV signals over actual velocity as a function of ω_c^* for zero pitch and yaw using the trigger scheme. (a) Measured over actual velocity. (b) r.m.s. variations in measured velocity over measurement volume, (c) proportion of measurement volume sensitive to each velocity.

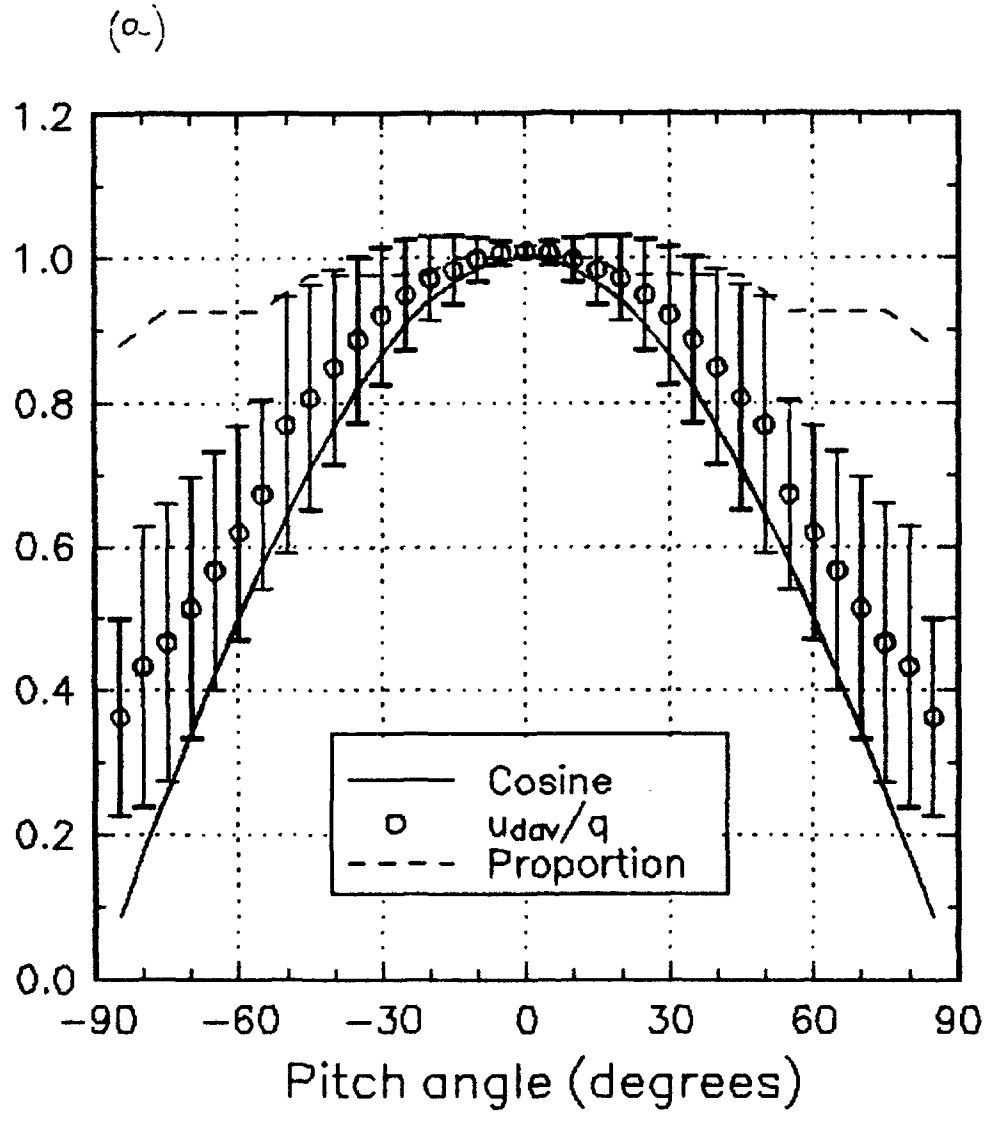

Figure 14. DAV angle response normalized on velocity at zero pitch and yaw, $\omega_c^* = 5.65$, trigger timing scheme for a trigger level of 0.1 and no discrimination level. Points show average over measurement volume, error bars show r.m.s. variation, dashed line shows proportion of measurement volume sensitive to each angle. (a) Pitch response, (b) yaw response.

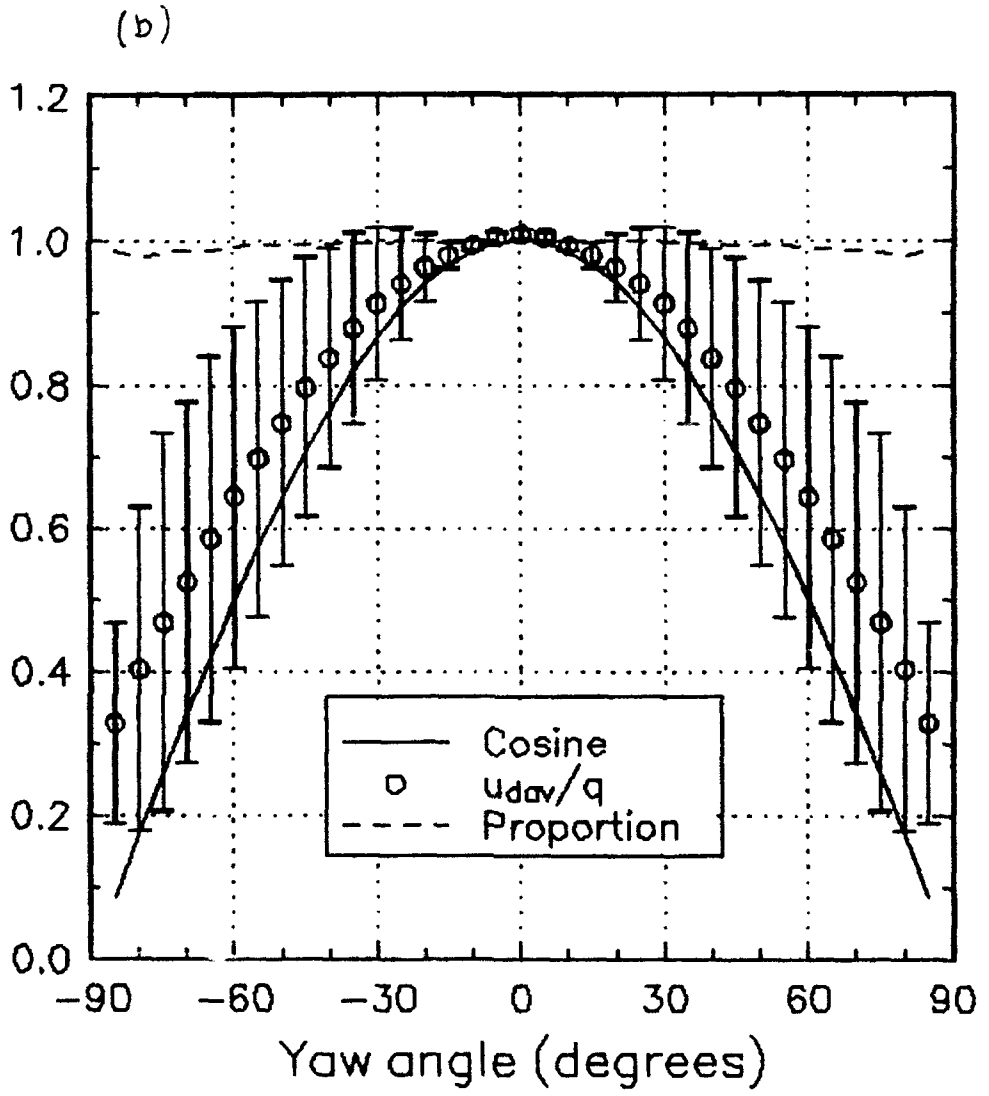

Figure 14. DAV angle response normalized on velocity at zero pitch and yaw, $\omega_c^* = 5.65$, trigger timing scheme for a trigger level of 0.1 and no discrimination level. Points show average over measurement volume, error bars show r.m.s. variation, dashed line shows proportion of measurement volume sensitive to each angle. (a) Pitch response, (b) yaw response.

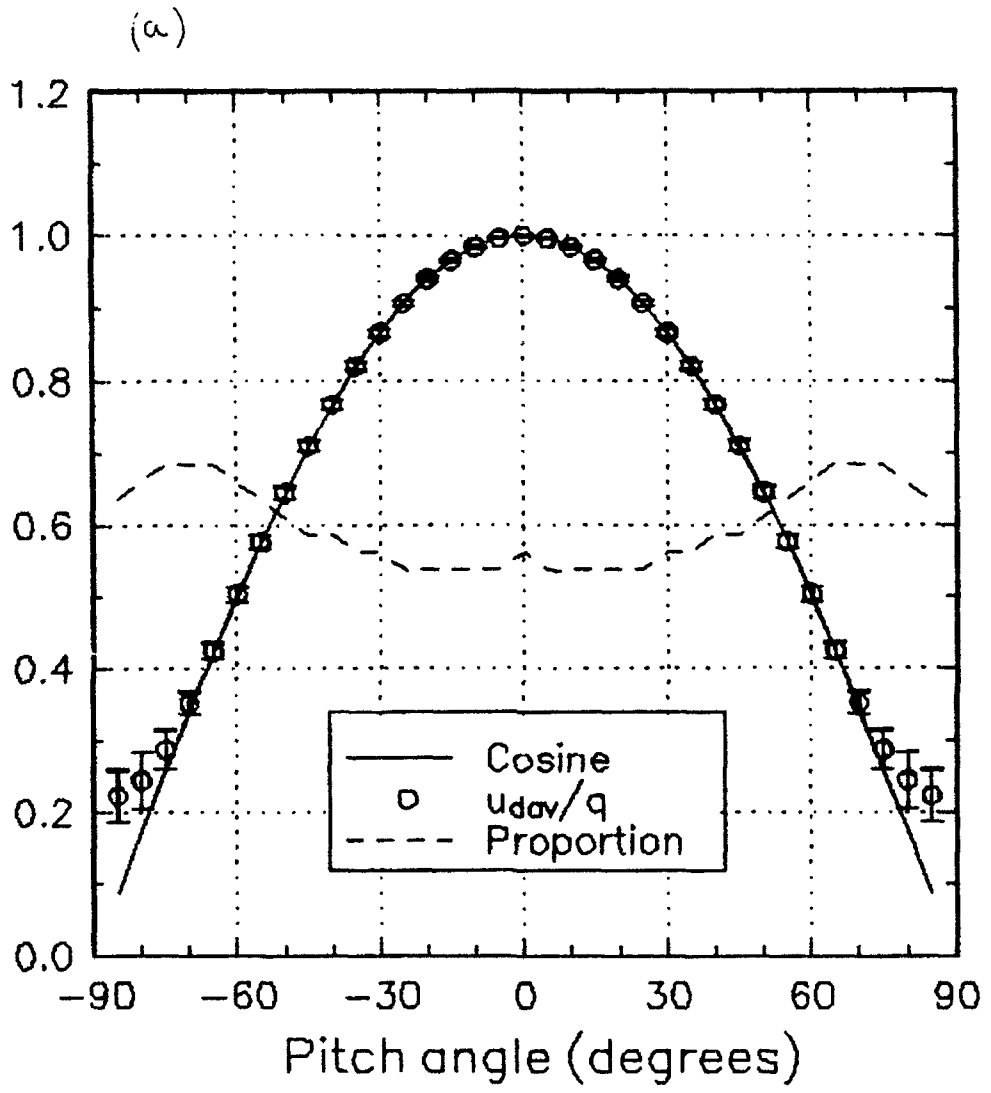

Figure 15. DAV angle response normalized on velocity at zero pitch and yaw, $\omega_c^* = 5.65$, trigger timing scheme for a trigger level of 0.1 and a discrimination level of 0.5. Points show average over measurement volume, error bars show r.m.s. variation, dashed line shows proportion of measurement volume sensitive to each angle. (a) Pitch response, (b) yaw response.

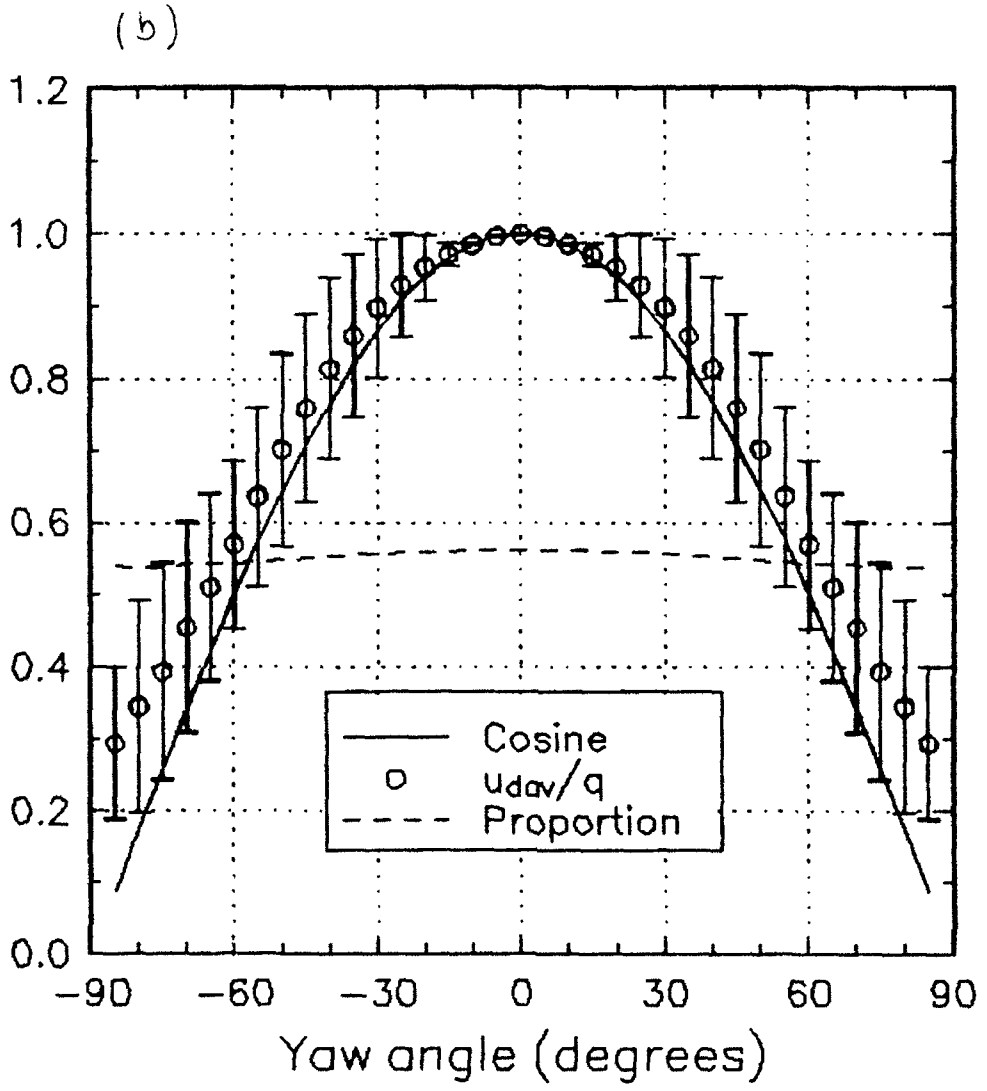

Figure 15. DAV angle response normalized on velocity at zero pitch and yaw, $\omega_c^* = 5.65$, trigger timing scheme for a trigger level of 0.1 and a discrimination level of 0.5. Points show average over measurement volume, error bars show r.m.s. variation, dashed line shows proportion of measurement volume sensitive to each angle. (a) Pitch response, (b) yaw response.

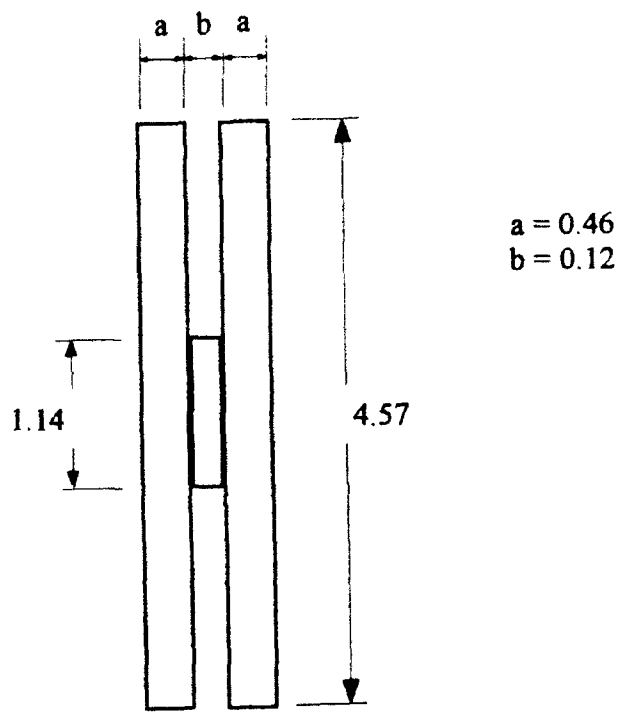

Figure 16. Improved photodiode array design. Dimensions are in mm and have been chosen assuming use of the same beam size and receiving lens magnification.

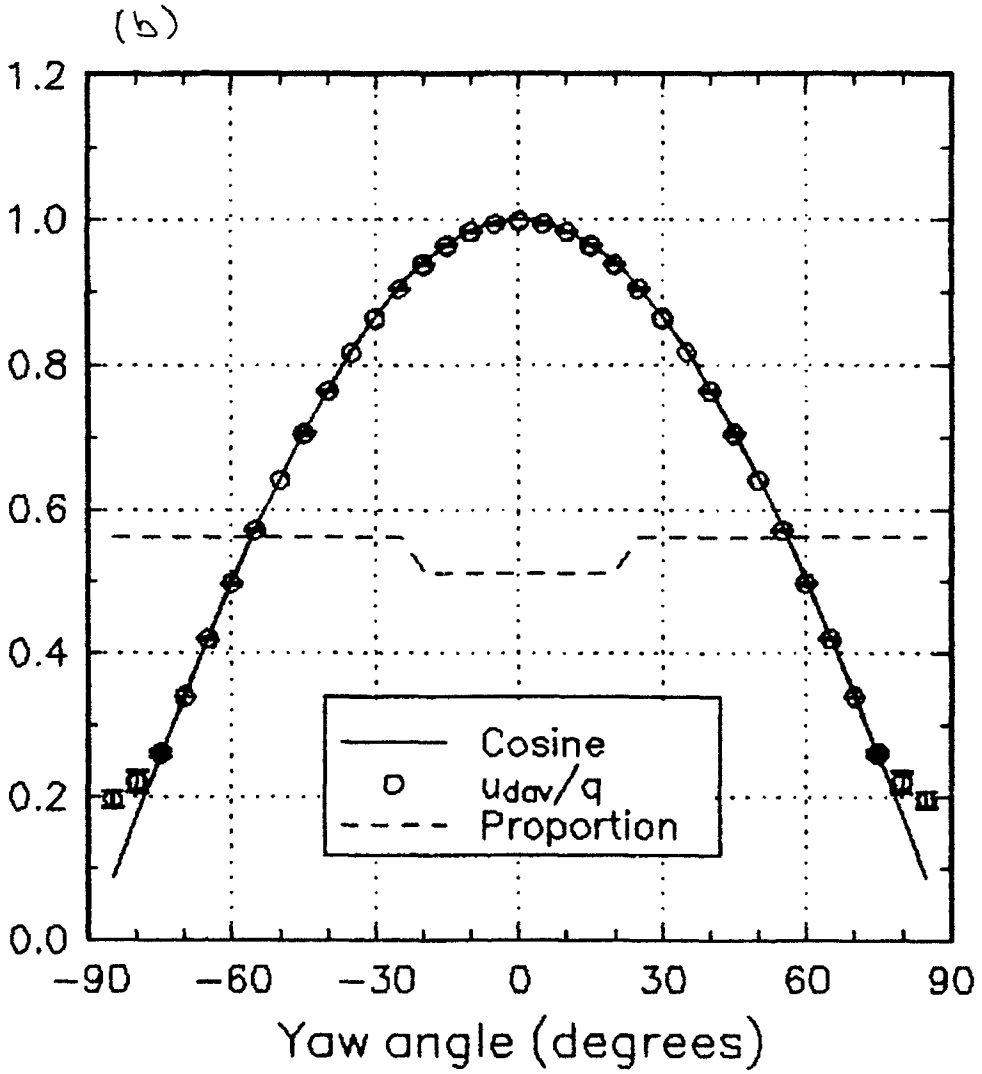

Figure 17. DAV angle response for the photodiode array design of figure 16. Response normalized on velocity at zero pitch and yaw, $\omega_c^* = 5.65$, trigger timing scheme for a trigger level of 0.1 and a discrimination level of 0.5. Points show average over measurement volume, error bars show r.m.s. variation, dashed line shows proportion of measurement volume sensitive to each angle. (a) Pitch response, (b) yaw response.

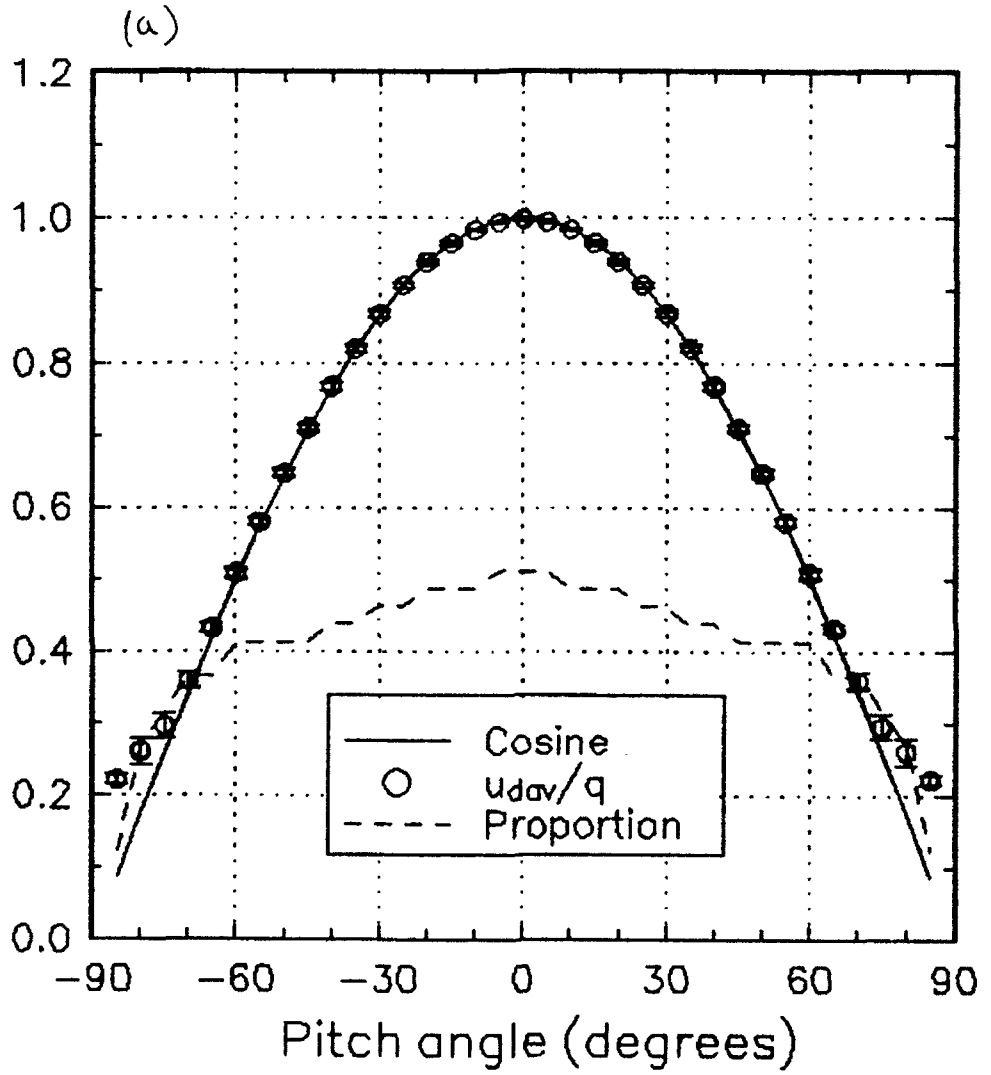

Figure 17. DAV angle response for the photodiode array design of figure 16. Response normalized on velocity at zero pitch and yaw, $\omega_c^* = 5.65$, trigger timing scheme for a trigger level of 0.1 and a discrimination level of 0.5. Points show average over measurement volume, error bars show r.m.s. variation, dashed line shows proportion of measurement volume sensitive to each angle. (a) Pitch response, (b) yaw response.

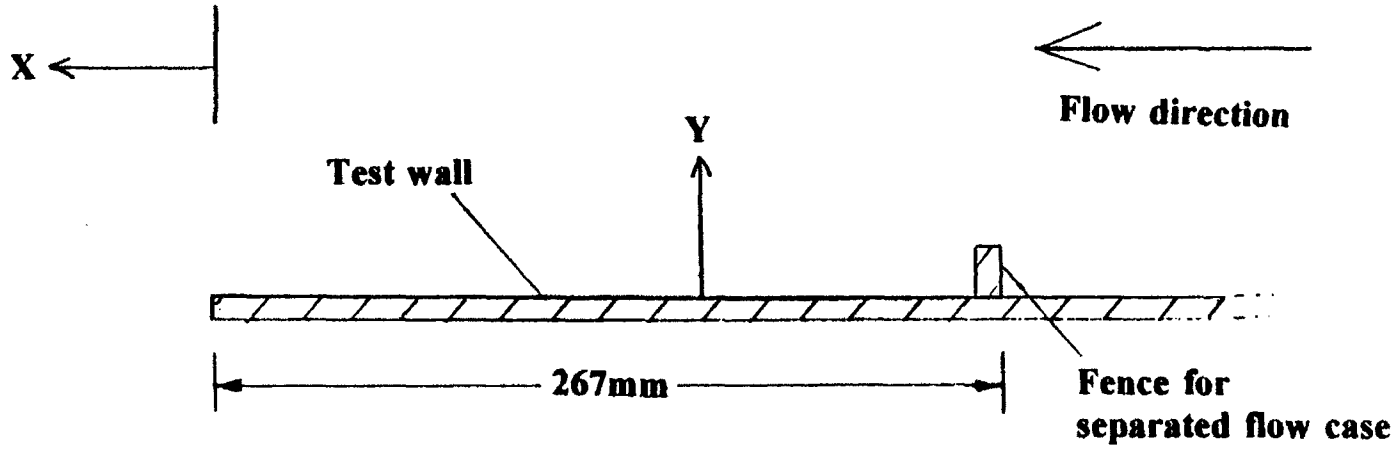

Figure 18. Schematic of the wind tunnel test section viewed in the Z direction.

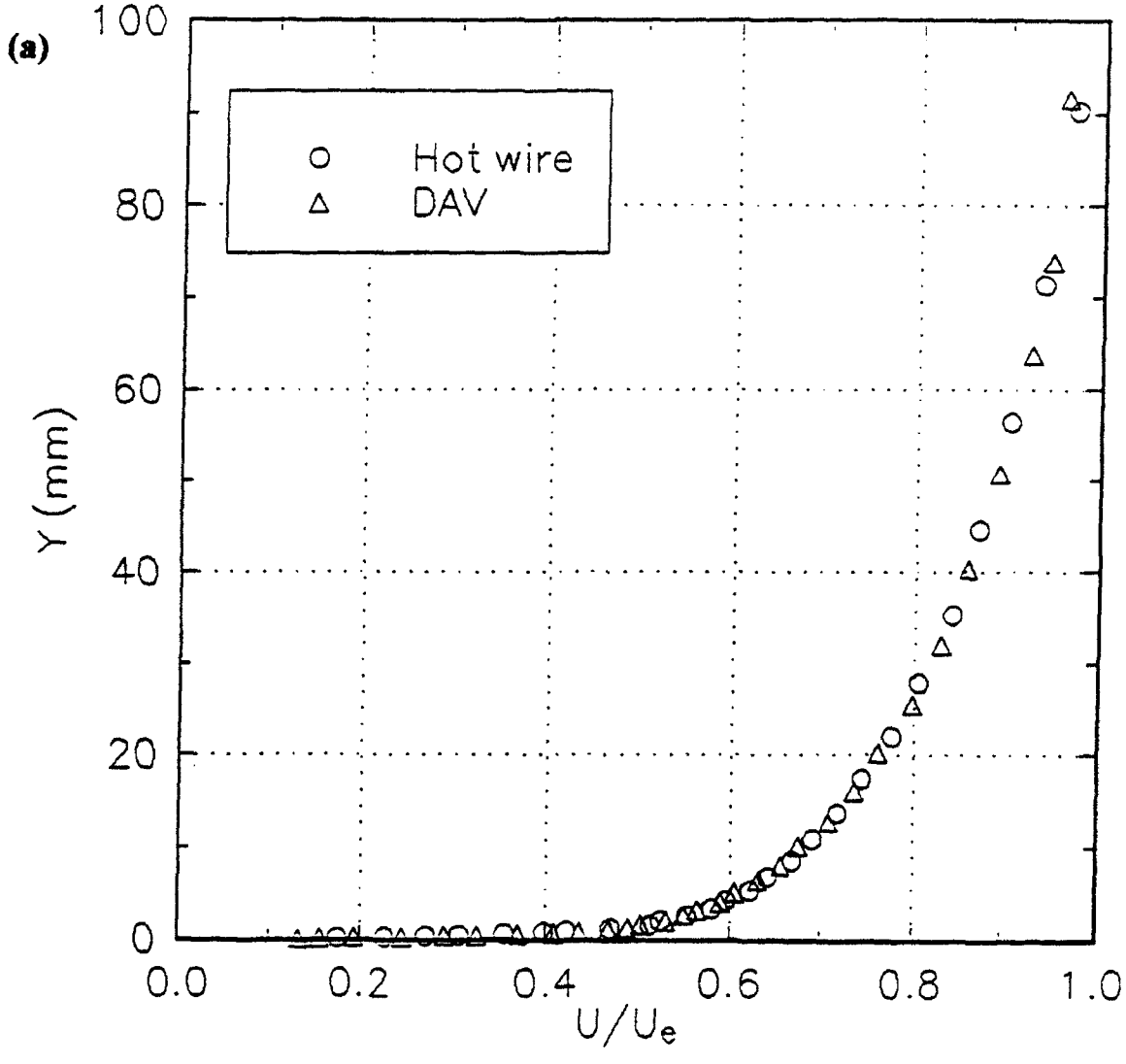

Figure 19. Velocity profiles for the turbulent boundary layer with U_e = 10m/s. (a) Mean velocity. (b) Mean velocity, solid line shows sublayer profile (friction velocity determined from slope of semi-log region). (c) Turbulence normal stress. (d) U skewness.

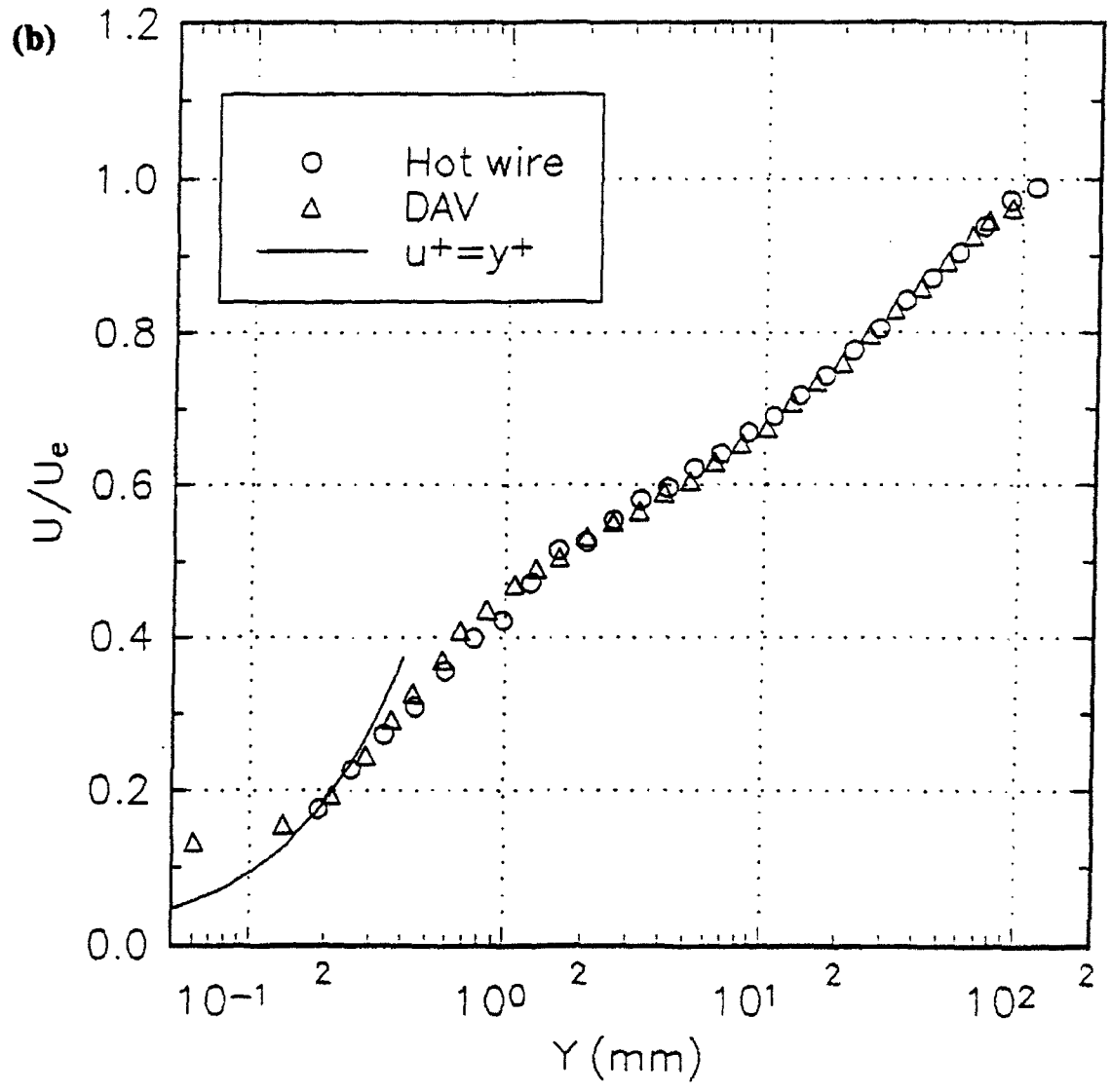

Figure 19. Velocity profiles for the turbulent boundary layer with U_e = 10m/s. (a) Mean velocity. (b) Mean velocity, solid line shows sublayer profile (friction velocity determined from slope of semi-log region). (c) Turbulence normal stress. (d) U skewness.

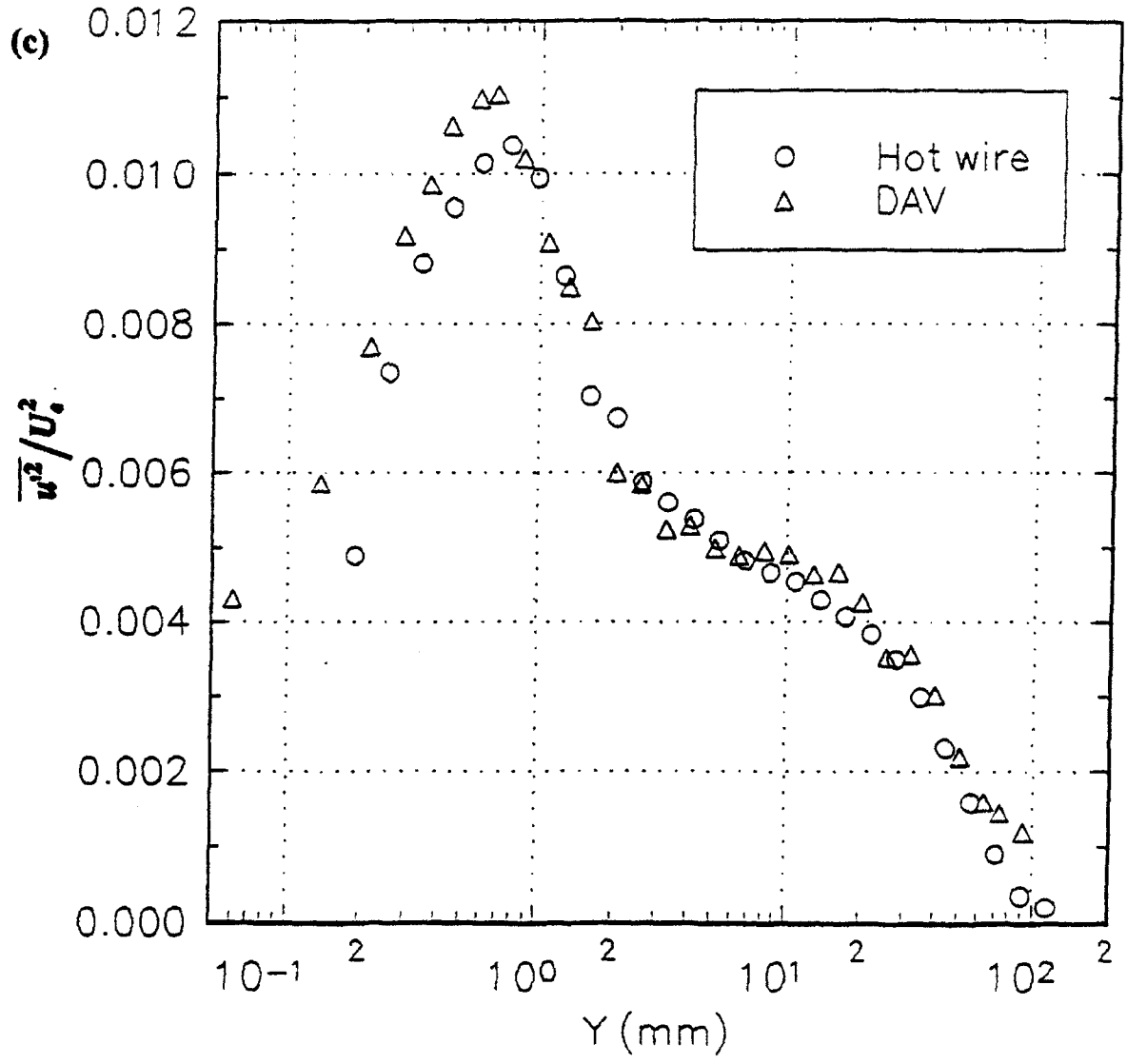

Figure 19. Velocity profiles for the turbulent boundary layer with U_e = 10m/s. (a) Mean velocity. (b) Mean velocity, solid line shows sublayer profile (friction velocity determined from slope of semi-log region). (c) Turbulence normal stress. (d) U skewness.

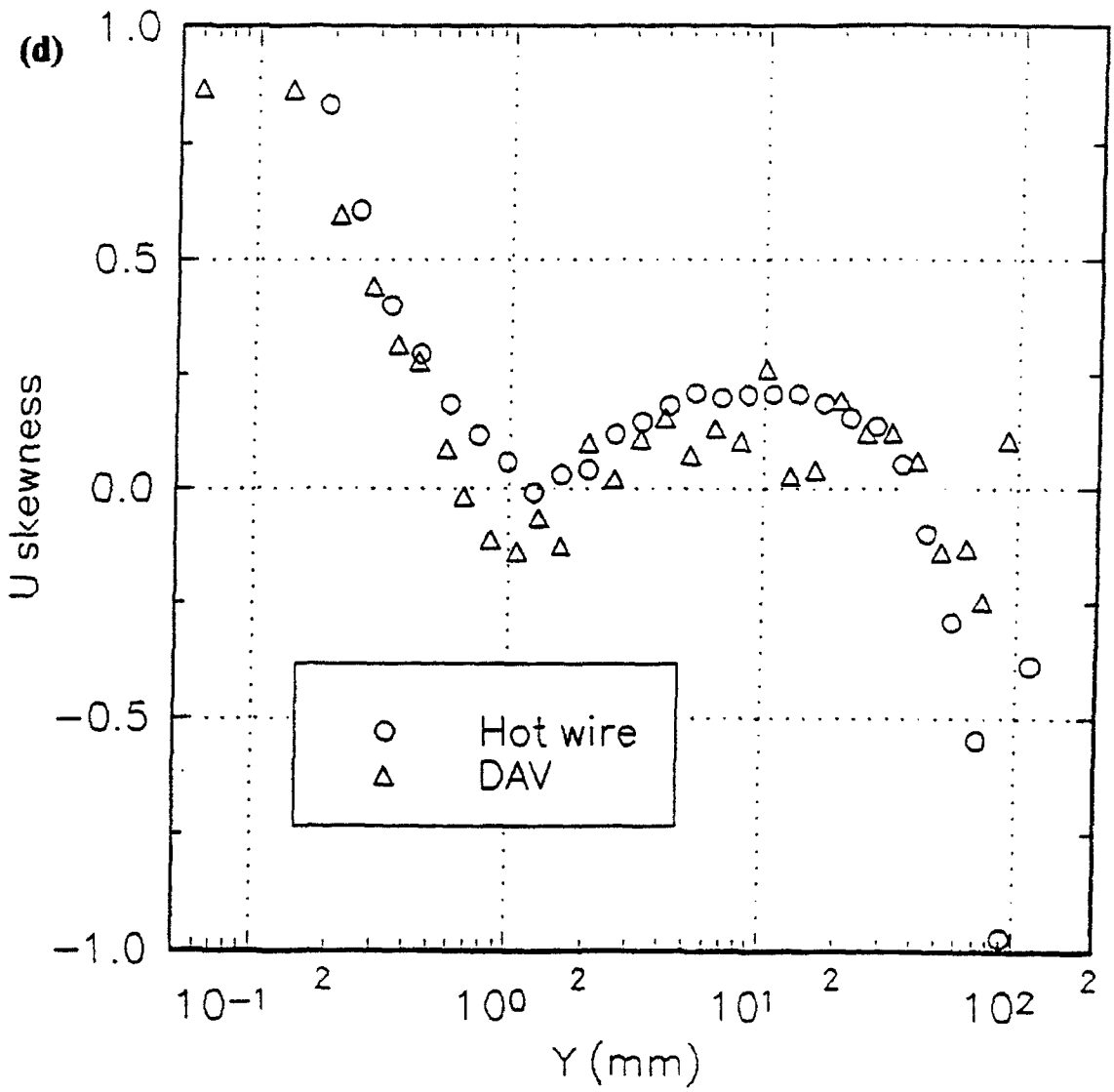

Figure 19. Velocity profiles for the turbulent boundary layer with U_e = 10m/s. (a) Mean velocity. (b) Mean velocity, solid line shows sublayer profile (friction velocity determined from slope of semi-log region). (c) Turbulence normal stress. (d) U skewness.

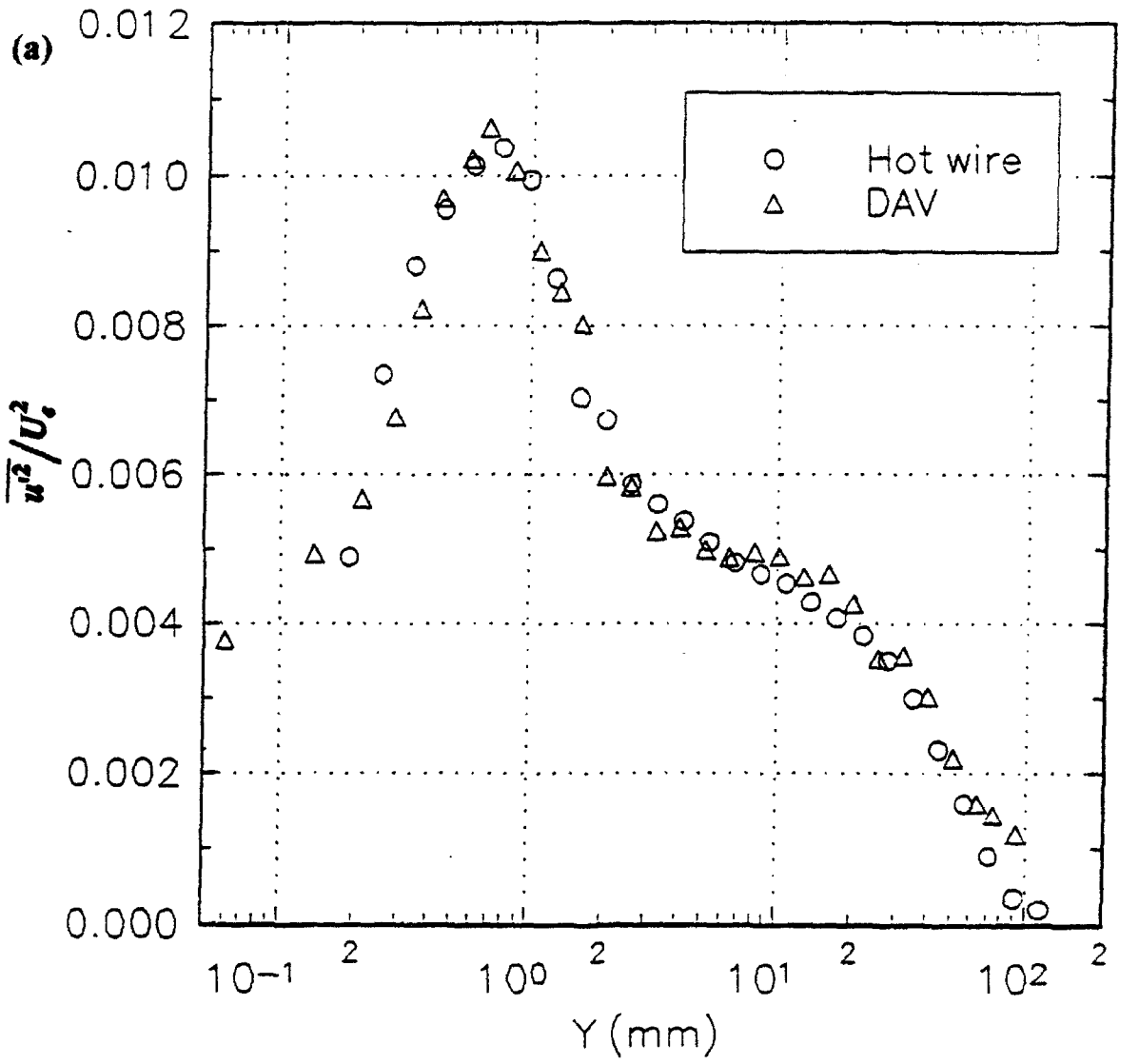

Figure 20. Velocity profiles for the turbulent boundary layer with U_e = 10m/s corrected for gradient broadening. (a) Turbulence normal stress. (b) U skewness.

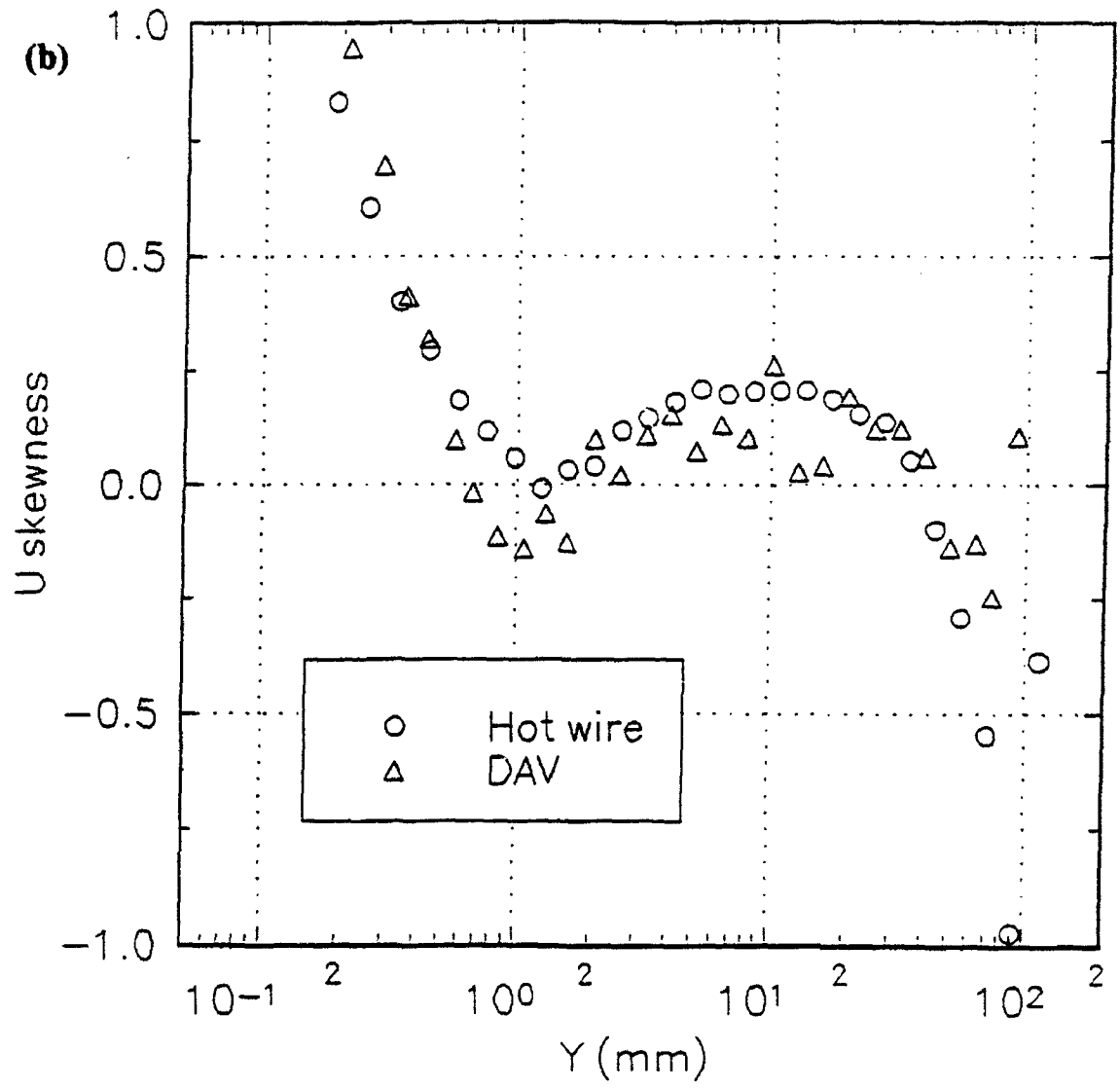

Figure 20. Velocity profiles for the turbulent boundary layer with U_e = 10m/s corrected for gradient broadening. (a) Turbulence normal stress. (b) U skewness.

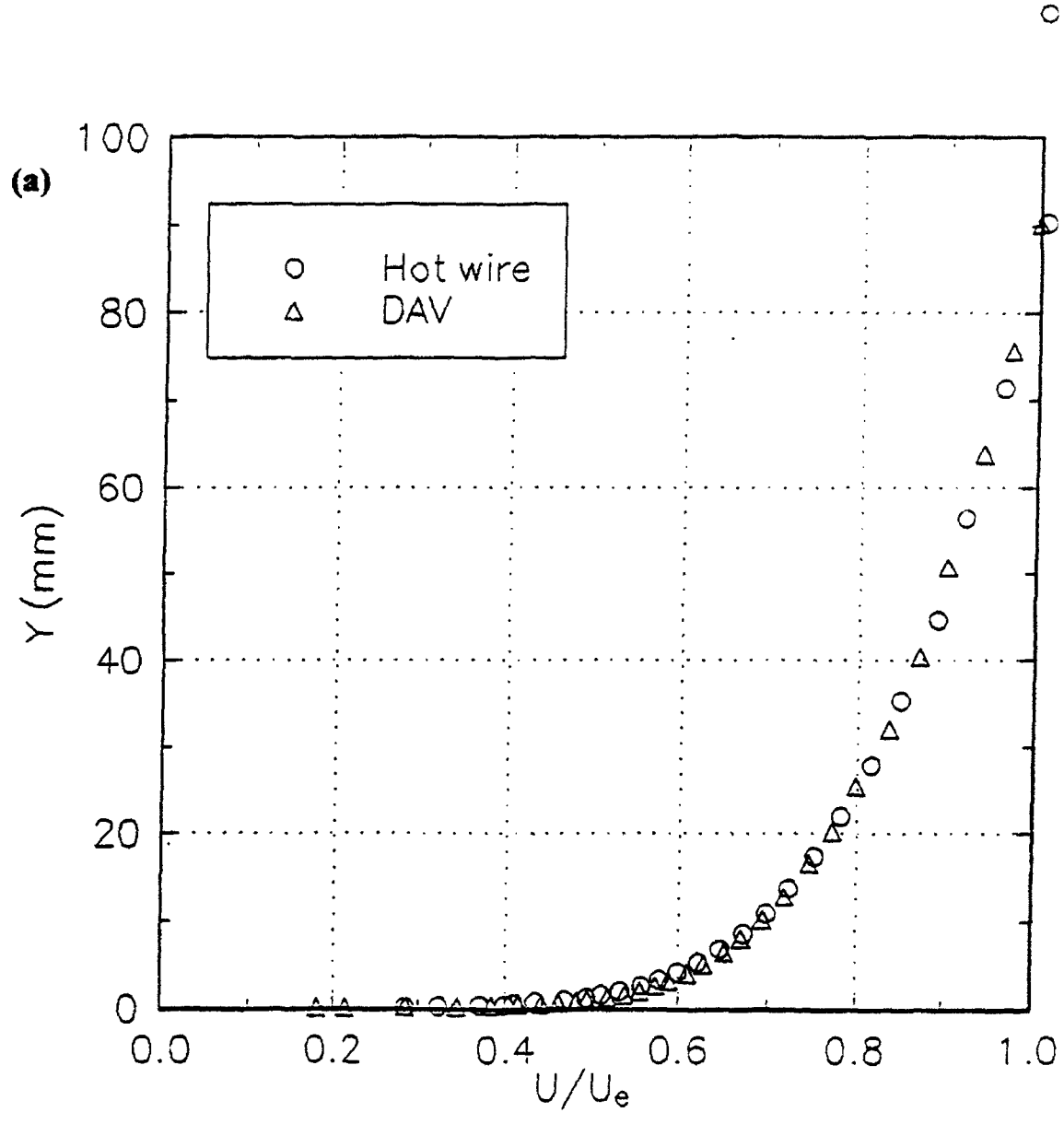

Figure 21. Velocity profiles for the turbulent boundary layer with U_e = 20m/s. (a) Mean velocity. (b) Mean velocity, solid line shows sublayer profile (friction velocity determined from slope of semi-log region). (c) Turbulence normal stress. (d) U skewness.

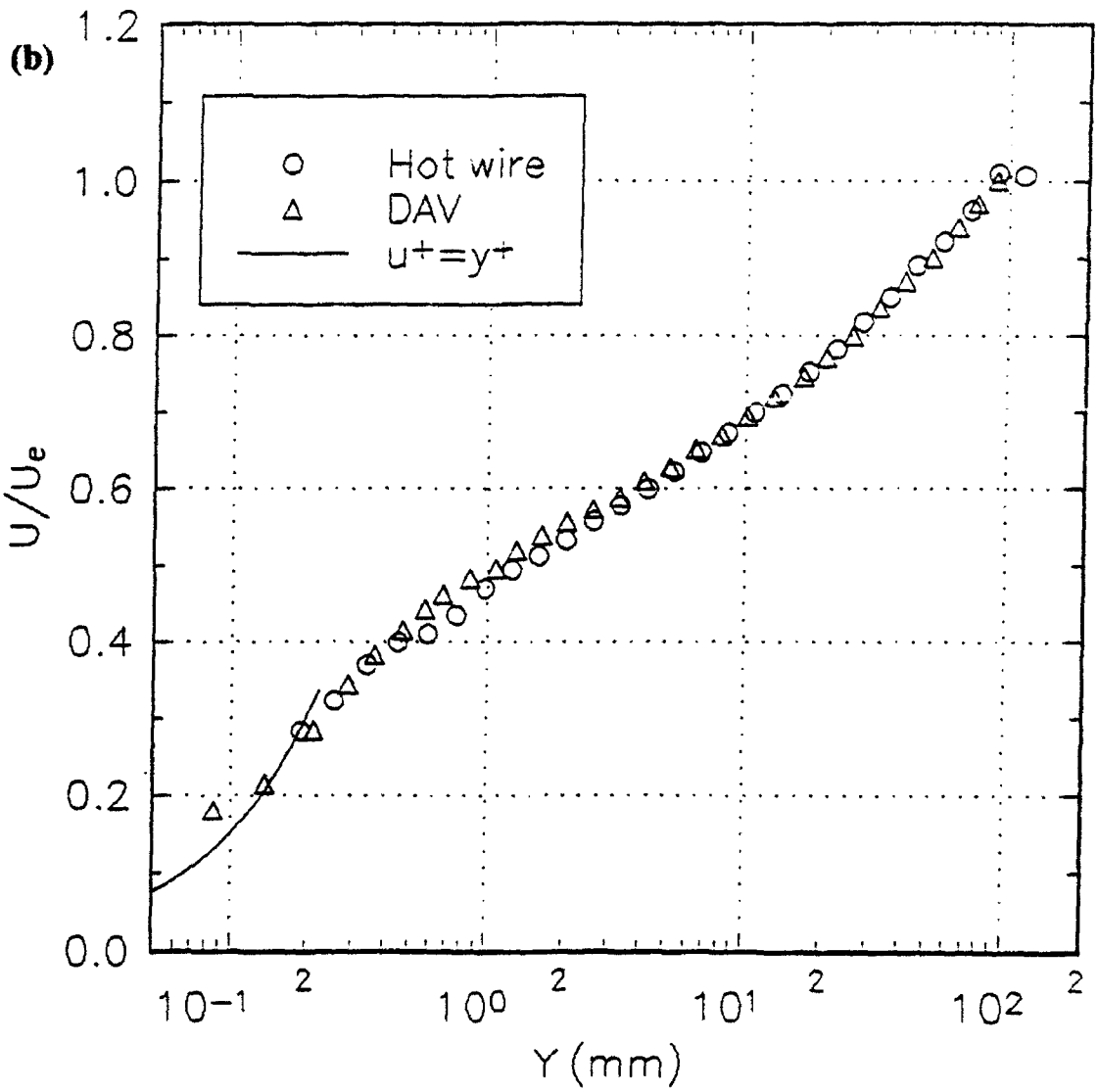

Figure 21. Velocity profiles for the turbulent boundary layer with U_e = 20m/s. (a) Mean velocity. (b) Mean velocity, solid line shows sublayer profile (friction velocity determined from slope of semi-log region). (c) Turbulence normal stress. (d) U skewness.

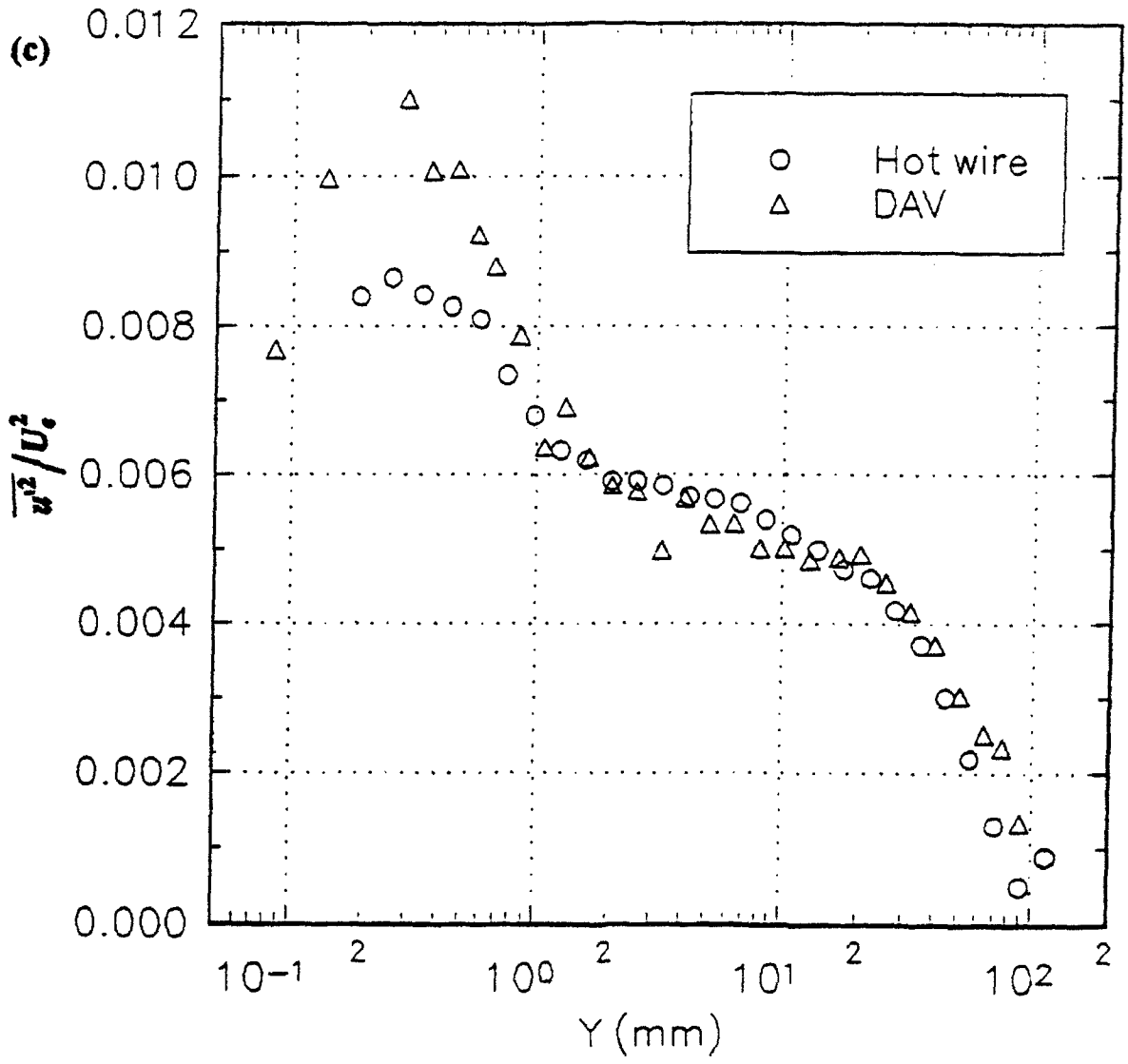

Figure 21. Velocity profiles for the turbulent boundary layer with U_e = 20m/s. (a) Mean velocity. (b) Mean velocity, solid line shows sublayer profile (friction velocity determined from slope of semi-log region). (c) Turbulence normal stress. (d) U skewness.

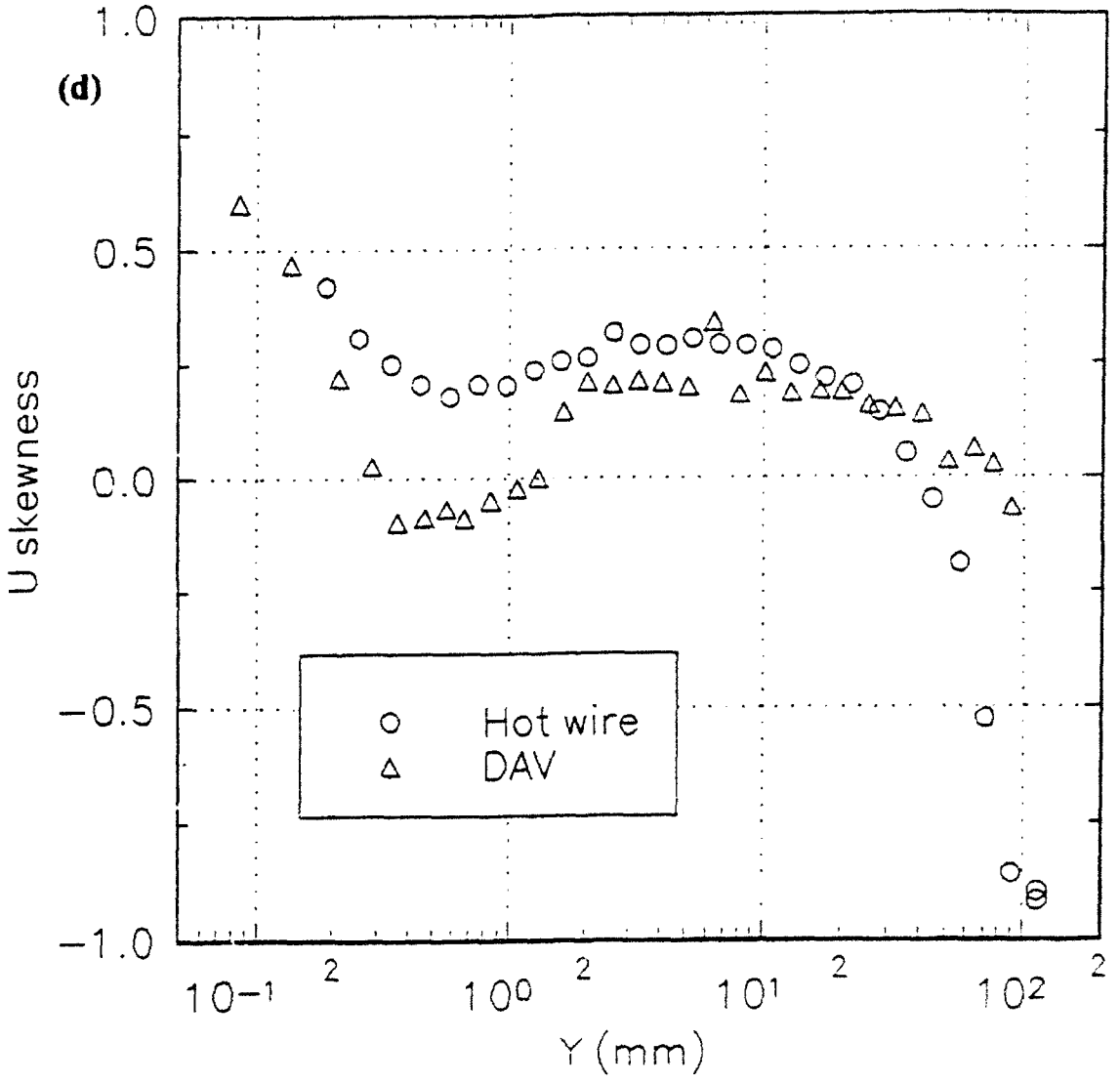

Figure 21. Velocity profiles for the turbulent boundary layer with U_e = 20m/s. (a) Mean velocity. (b) Mean velocity, solid line shows sublayer profile (friction velocity determined from slope of semi-log region). (c) Turbulence normal stress. (d) U skewness.

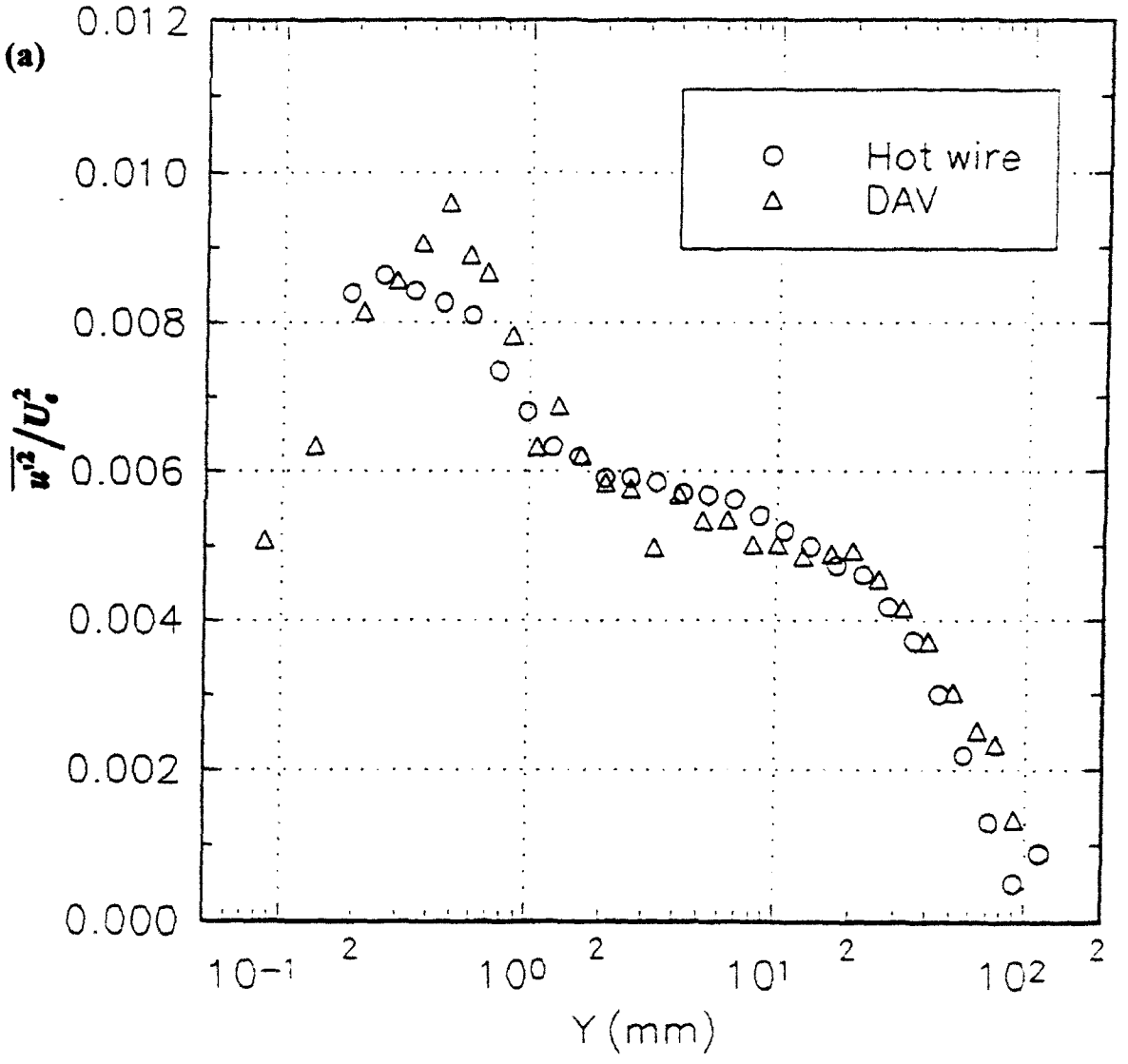

Figure 22. Velocity profiles for the turbulent boundary layer with U_e = 20m/s corrected for gradient broadening. (a) Turbulence normal stress. (b) U skewness.

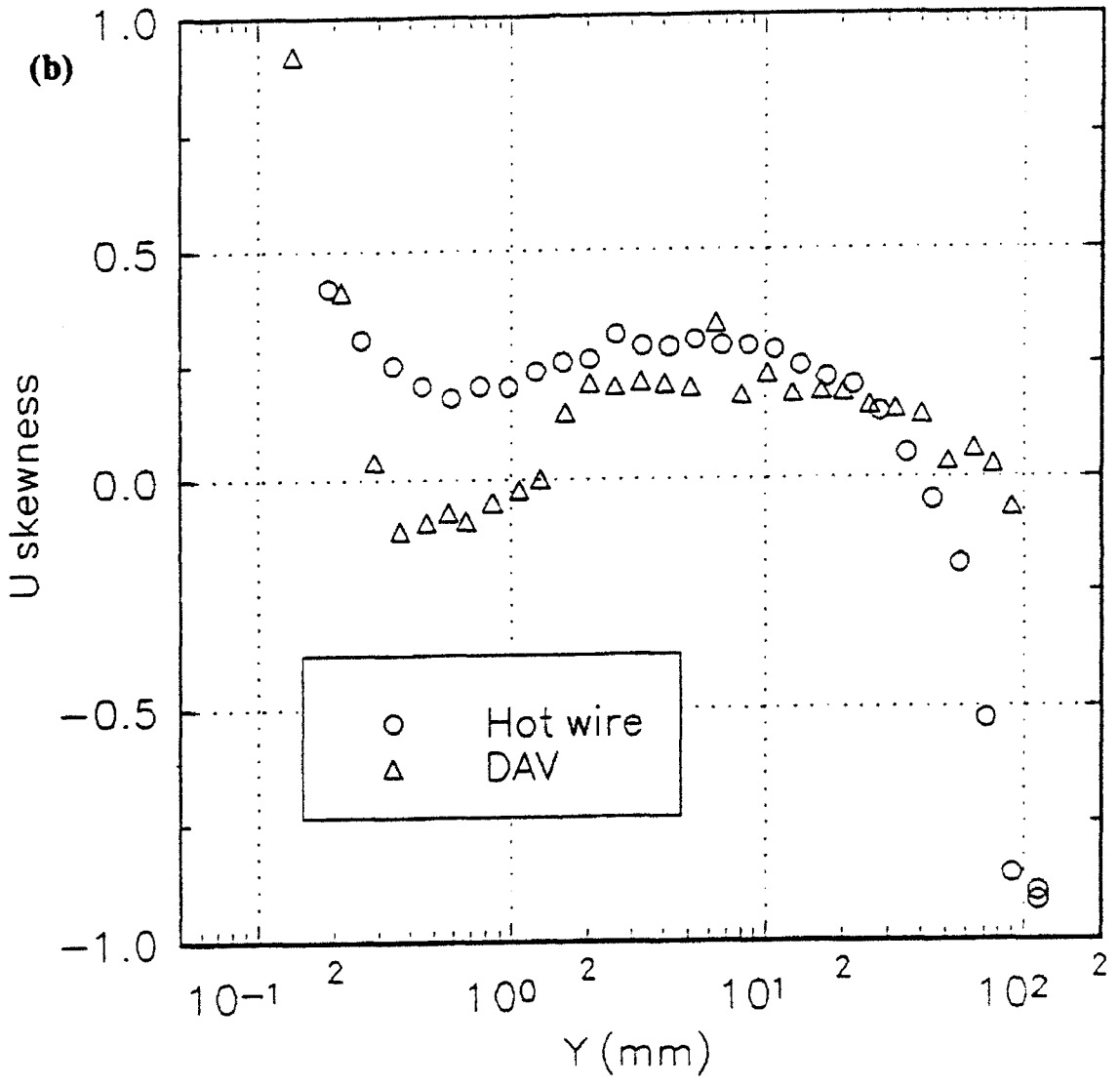

Figure 22. Velocity profiles for the turbulent boundary layer with U_e = 20m/s corrected for gradient broadening. (a) Turbulence normal stress. (b) U skewness.

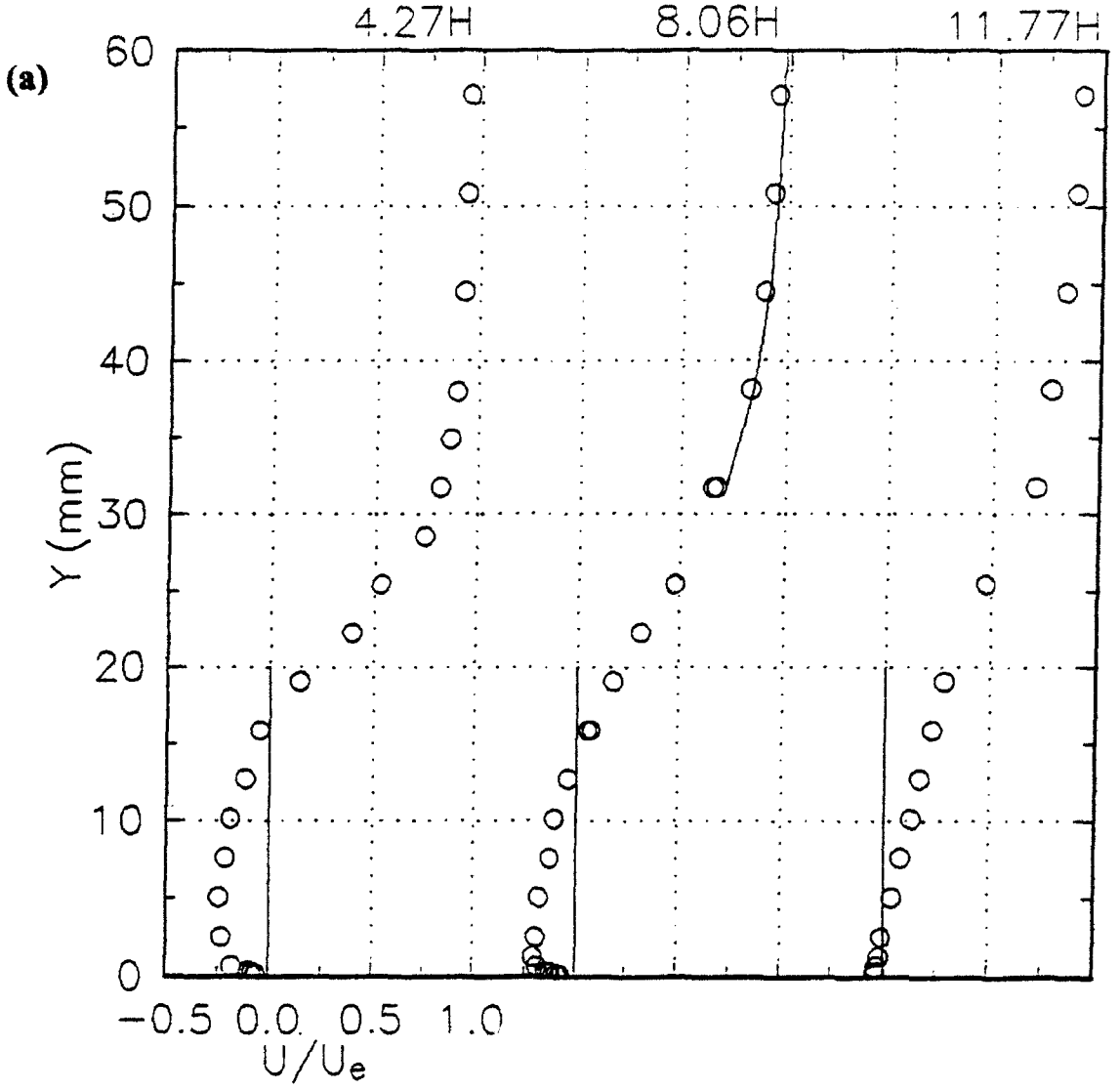

Figure 23. (a) Mean velocity profiles measured in the separated flow at X=-213mm , -165mm, and -117mm corresponding respectively to 4.27, 8.06 and 11.77H from separation. Solid line shows hot-wire measurements. (b) Detail of near-wall region.

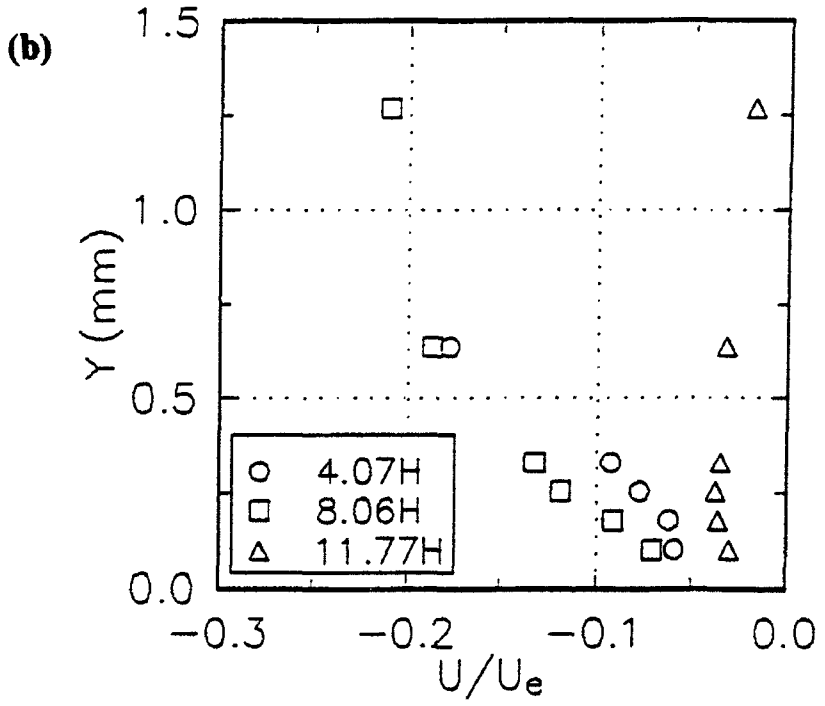

Figure 23. (a) Mean velocity profiles measured in the separated flow at X=-213mm , -165mm, and -117mm corresponding respectively to 4.27, 8.06 and 11.77H from separation. Solid line shows hot-wire measurements. (b) Detail of near-wall region.

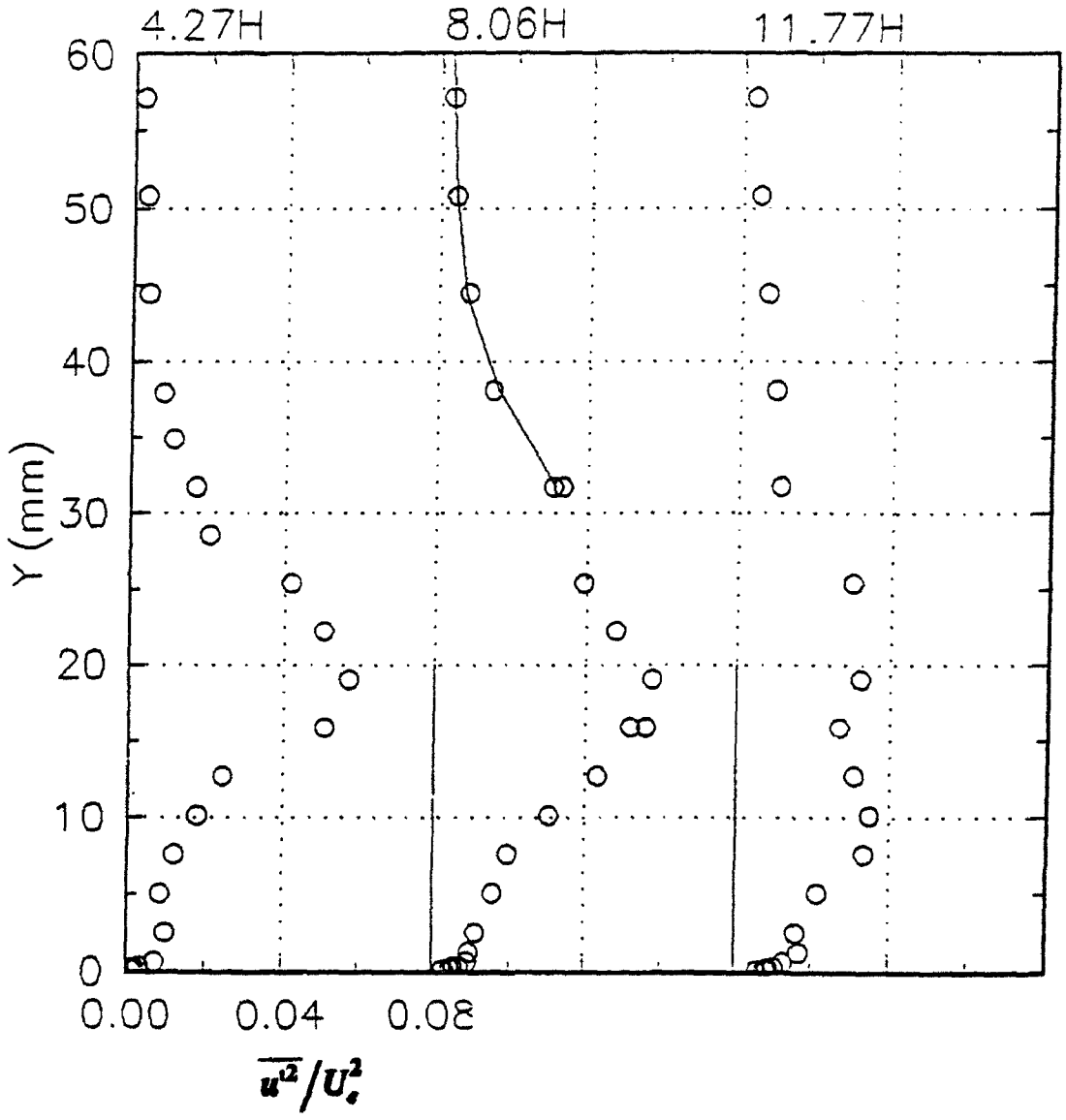

Figure 24. Turbulence normal stress profiles measured in the separated flow at X=-213mm , -165mm, and -117mm corresponding respectively to 4.27, 8.06 and 11.77H from separation. Solid line shows hot-wire measurements.

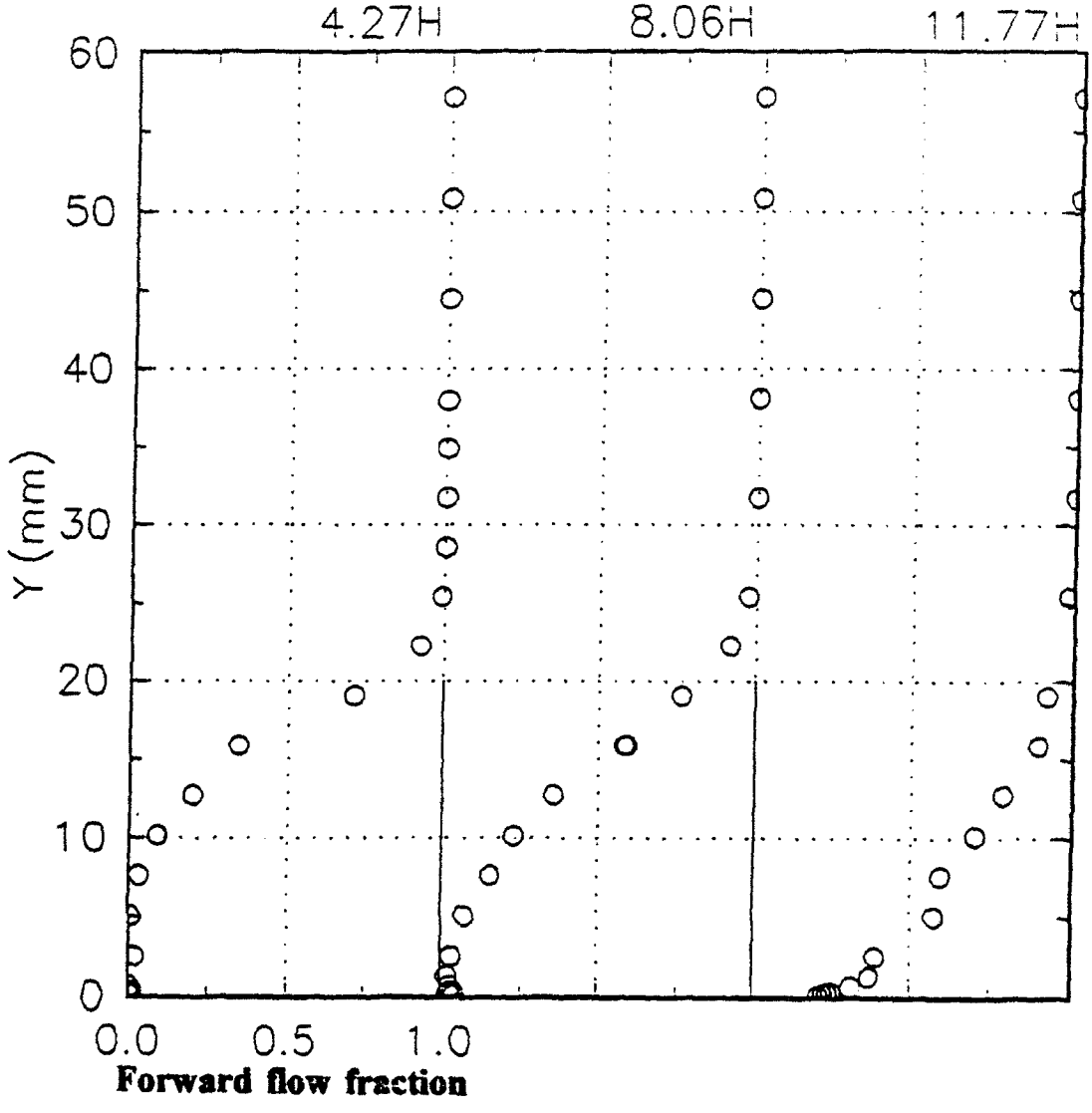

Figure 25. Forward-flow fraction profiles measured in the separated flow at X=-213mm , -165mm, and -117mm corresponding respectively to 4.27, 8.06 and 11.77H from separation.

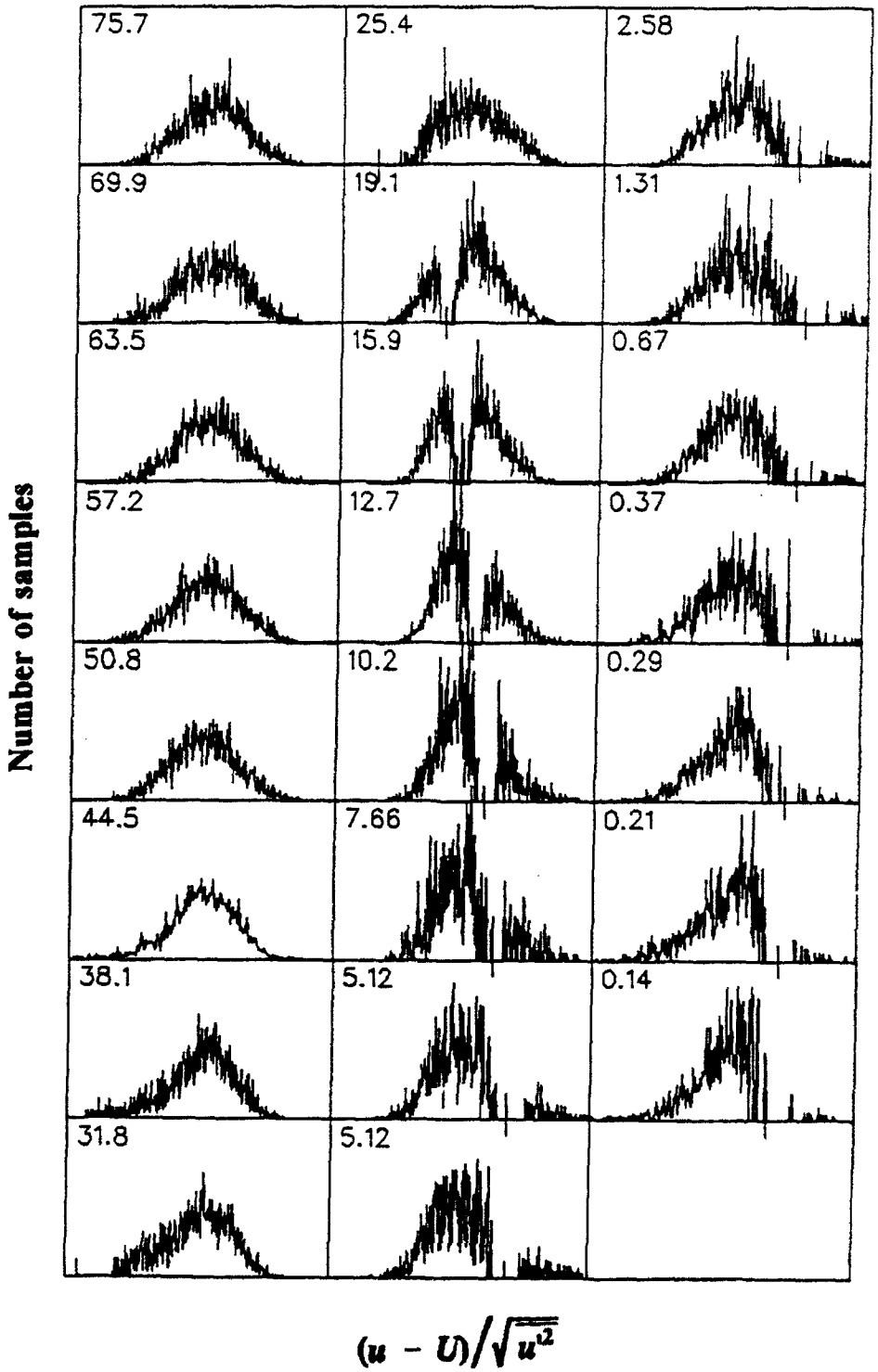

Figure 26. Sequence of histograms measured at X=-165mm. Number in top left hand corner of each histogram indicates y location in mm. Tick on horizontal axes indicates location of zero velocity.

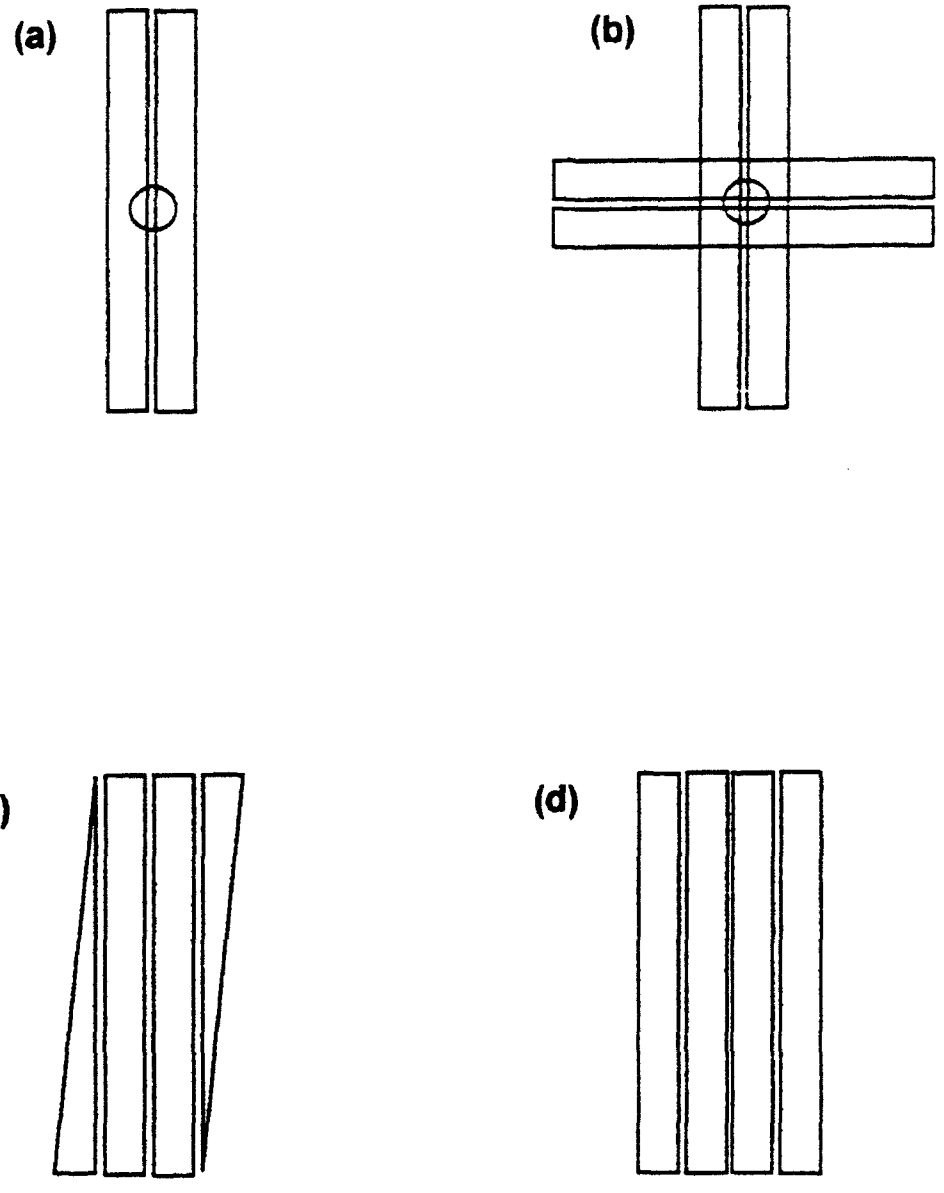

Figure 27. Some proposed photodiode array designs. (a) For improved accuracy in one-component measurements (circular element is optically overlaid on rectangular elements) (b) for two-component velocity measurements from one receiving angle (rectangular and circular elements overlaid) (c) for one-component velocity and position measurements (d) for multiple velocity measurements of the same particle.